CHAPTER

3

METHODS UTILIZING LOW AND MEDIUM LASER IRRADIANCE

A. LASER-INDUCED THERMAL DESORPTION AND MATRIX-ASSISTED METHODS

AKOS VERTES

Department of Chemistry
George Washington University
Washington, D.C.

RENAAT GIJBELS

Department of Chemistry
University of Antwerp (UIA)
Antwerp, Belgium

3A.1. INTRODUCTION

Producing ions from large molecules is of marked importance in mass spectrometry. In this chapter we survey different laser desorption methods in view of their virtues and drawbacks in volatilization and ion generation. Laser-induced thermal desorption and matrix-assisted laser desorption are assessed with special emphasis on the recent breakthrough in the field ($m/z > 100{,}000$ ions produced by matrix-assisted laser desorption). Efforts to understand and describe laser desorption and ionization are also discussed. We emphasize the role of restricted energy transfer pathways as a possible explanation for the volatilization of nondegraded large molecules.

With the growing importance of biomedical investigations in organic analysis, the emphasis has been shifting to the detection and structure determination of ever larger and more complex molecules. Gas phase analytical methods in general—and mass spectrometry was not an exception—exhibited

Laser Ionization Mass Analysis, Edited by Akos Vertes, Renaat Gijbels, and Fred Adams. Chemical Analysis Series, Vol. 124.
ISBN 0-471-53673-3

increasing difficulties with these larger and larger molecular masses because of the involatility and instability of such materials.

The early answer to this challenge came in the 1970s, in the form of so-called soft ionization techniques. Field desorption, chemical ionization, plasma desorption, secondary ion, electrohydrodynamic, and laser desorption ion sources were developed to cope with nonvolatile compounds. A thorough overview of these methods with respect to their high mass capabilities was published by Daves 1979. There seemed to be two distinct strategies to follow: (a) optimization of volatilization conditions in terms of sample dispersion and heating rate; or (b) direct ionization of molecules from a surface by external electrostatic field, particle bombardment, or laser radiation. At this stage of development, however, analytical possibilities were limited to the mass range $m/z < 10{,}000$.

During the 1980s four techniques were able to overcome this limit: ^{252}Cf plasma desorption mass spectrometry (Sundqvist and Macfarlane, 1985) became available in the $m/z < 45{,}000$ mass range; fast atom bombardment (FAB)—an offspring of secondary ionization with special sample preparation—reached the $m/z \approx 24{,}000$ region (Barber and Green, 1987); the two forerunners, however, became electrospray ionization (Fenn et al., 1990) and matrix-assisted laser desorption (MALD) (Karas et al., 1989a), with $m/z = 133{,}000$ and $m/z = 250{,}000$ high mass records, respectively. The latest developments indicate capabilities for both techniques even beyond these limits (Nohmi and Fenn, 1990; Williams and Nelson, 1990).

The primary information stemming from MALD and electrospray measurements is the mass-to-charge ratio (m/z) of the molecular ions. It is the quick and accurate determination of molecular weight that makes these methods especially attractive. However, one should not overemphasize the value of molecular weight determination by these methods. Several other long-established techniques are available in the same or even in a broader molecular weight range. Ultracentrifugation, light scattering, gel permeation chromatography, and gel electrophoresis cover the molecular weight region from ~ 1000 to $\sim 5{,}000{,}000$ (Siggia, 1968). The cost and availability of the necessary instrumentation compares favorably to mass spectrometric equipment. When assessing the different molecular weight determination methods it is necessary to keep in mind that mass spectrometry directly provides mass-to-charge ratio data, whereas the separation techniques measure particle mobilities and may incorporate systematic errors.

An important aspect of the analytical value of mass spectrometric methods is their remarkably high sensitivities and low detection limits. Recent reports on electrospray ionization put sensitivities in the low picomole per microliter region and detection limits in the low femtomole region for several 556 <

$m/z < 66{,}000$ peptides (Van Berkel et al., 1990). Both sensitivity and detection limits, however, are highly compound dependent. The detection limit increases with increasing molecular weight, because the ion signal is distributed over more charged states (Loo et al., 1990).

Similar, or even better results were obtained with laser desorption. The sensitivity was in the low picomole per microliter region, whereas the detection limits were in the subpicomole (Karas et al., 1990a: $10{,}000 < m/z < 100{,}000$ peptides) or in the subfemtomole region (Hahn et al., 1987: for porphyrin derivatives).

Naturally, these numbers should be evaluated with the achievements of other techniques in mind. As an example, we cite here some results on the analytical performance of open tubular liquid chromatography. As little as 4 fmol protein was hydrolyzed and derivatized, resulting in approximately 25 nL volume analyte solution. In this mixture quantitative determination of 14 amino acid constituents was carried out with about 5% error (Oates and Jorgenson, 1990). Chromatographic and immunoassay analyses are serious competitors in terms of sensitivity, with usually much lower instrumentation costs and consequently with better availability.

Efforts to volatilize large molecules and detect minute quantities with the aid of lasers and mass spectrometry will be the topic of this section. Laser desorption mass spectrometry of nonvolatile organic molecules was surveyed by Shibanov (1986), but vigorous development in the field since then has changed the landscape considerably.

We will focus our attention on what the different laser desorption and ionization methods have to offer over the capabilities of the more widespread analytical tools. Special emphasis will be given to the mass range and mass accuracy, to detection limits and sensitivity, to the freedom from matrix interferences, and to the availability of structural information. Two types of experiments will be examined in separate sections: laser-induced thermal desorption in Section 3A.2, and matrix-assisted laser desorption in Section 3A.4. Between these discussions, Section 3A.3 presents some theoretical considerations on the laser irradiance threshold for plume formation. The growing number of applications have made it necessary to discuss the MALD analysis of biological molecules separately. This is the subject of Section 3A.5.

In Section 3A.6 we survey and comment on the existing ideas and models that seek to explain laser desorption of large molecules. The concepts range from rapid heating (Beuhler et al., 1974) to mechanical approaches (Williams, 1990), to restricted energy transfer (Vertes and Gijbels, 1991), to expansion cooling of the laser-generated plume (Vertes, 1991b). The short final section is devoted to our present understanding of ion formation processes in MALD.

3A.2. LASER-INDUCED THERMAL DESORPTION

The idea of laser-induced thermal desorption (LITD) stems from early studies of the influence of laser radiation on small molecules adsorbed on solid surfaces. If the substrate absorbs the laser radiation, it heats up on a time scale comparable to the laser pulse length. The resulting temperature rise leads to the detachment of the adsorbed molecules.

It was soon realized that Q-switched laser pulses (whose durations are on the nanosecond time scale) may lead to subthermal velocity distributions of the desorbed particles (Wedler and Ruhmann, 1982). Further studies suggested that the desorption process is adiabatic, especially in the case of monolayers (Simpson and Hardy, 1986).

The possibility of desorbing cold molecules from hot surfaces seemed very promising and triggered studies on larger molecules. The conflict of volatilization vs. thermal lability of these compounds was thought to be overcome (van der Peyl et al., 1982a). Calculated surface temperatures showed strong correlation with the generated ion currents. The effort to implement the method for higher mass compounds, however, was apparently not completely successful: $m/z \approx 10{,}000$ seemed to be an upper limit of ion production by LITD (Ijames and Wilkins, 1988).

Clearly, the evolution of substrate surface temperature plays a decisive role in the course of events in LITD (Vertes et al., 1989b). Temporal and spatial temperature distributions, $T(\mathbf{r}, t)$, in the substrate can be described by the heat conduction equations:

$$C(T)\frac{\partial T(\mathbf{r}, t)}{\partial t} = -\operatorname{div} J(\mathbf{r}, t) + I(\mathbf{r}, t) \tag{1}$$

and

$$J(\mathbf{r}, t) = K(T)\nabla T(\mathbf{r}, t) \tag{2}$$

where $I(\mathbf{r}, t)$ is the source term describing the laser heating and $J(\mathbf{r}, t)$ is the heat flow; $C(T)$ and $K(T)$ are the specific heat and the heat conductivity, respectively, generally exhibiting considerable temperature dependence. The source term can be expressed in terms of laser irradiance, $I_0(\mathbf{r}, t)$, corrected for surface reflection, R:

$$I(\mathbf{r}, t) = \alpha(1 - R)I_0(\mathbf{r}, t)\exp[-\alpha z) \tag{3}$$

where the light propagates along the z-axis perpendicular to the substrate surface; α is the light absorption coefficient of the substrate at the laser wavelength.

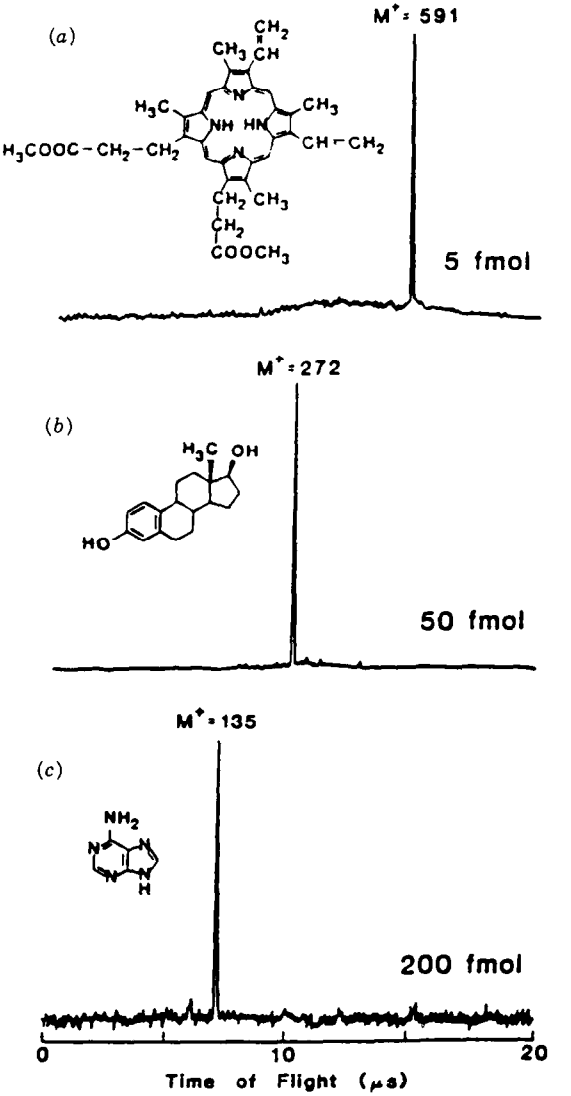

Figure 3A.1. Laser desorption–multiphoton ionization mass spectra of (a) protoporphyrin IX dimethyl ester, (b) β-estradiol, and (c) adenine. The amount of each sample desorbed by a CO_2 laser pulse is 5, 50, and 200 fmol, respectively. Operating conditions: CO_2 laser fluence, $\sim 400\,mJ/cm^2$; Nd:YAG laser fluence, $\sim 3\,mJ/cm^2$; duty cycle = 10 Hz, and signal averaging time = 20 s. From Hahn et al. (1987) with permission of the American Chemical Society.

The solution of the linear problem (K and C being constant) for general laser intensity distributions and for the special case of a Gaussian beam was found by Lax (1977). The non linear problem of temperature-dependent heat conductivity was also solved analytically (Lax, 1978).

Experimental results also became available to trace surface temperature rise as the consequence of a laser pulse. The resistance change of a vapor-deposited platinum stripe on an insulating substrate provided time-resolved information on surface heating (Zenobi et al., 1988). Comparison of the measured temperatures with analytical solutions of Eqs. (1)–(3) in the linear, one-dimensional case and with numerical solutions in the nonlinear case concluded in favor of the latter (Philippoz et al., 1989).

Both experiments and calculations indicated extremely high heating rates, generally in excess of 10^8 K/s. In a study of surface decomposition, the kinetics of reaction and desorption were considered to be competing first-order processes (Deckert and George, 1987). It was possible to show the existence of a crossover point of the product yield curves, indicating the takeover of desorption.

Analytical applications of LITD excel in particularly low detection limits. In the case of protoporphyrin IX dimethyl ester, subfemtomolar quantities of the analyte provided detectable signals ($S/N = 2$) (Hahn et al., 1987). Figure 3A.1 shows molecular ion signals for three compounds utilizing femtomolar quantities of sample. The molecules were desorbed by a CO_2 laser pulse, and subsequently ionized by a frequency-quadrupoled Nd:YAG laser. Ion detection was carried out by a time-of-flight mass spectrometer. Linear dependence of the parent ion signal intensity with adsorbate concentration was found over a range of 5 orders of magnitude (Zare et al., 1988), offering remarkable quantitation possibilities.

3A.3. THE IRRADIANCE THRESHOLD FOR PLUME FORMATION

As laser irradiance increases, laser desorption—characterized alone by energy transfer across the steady surface and by occasional detachment of particles—gives rise to plume formation. To see all forms of laser–solid interaction it is important to realize that even for a given material there are several different regimes depending on the laser irradiance. The simplest case involves the following possibilities:

a. Surface heating with thermal desorption
b. Surface melting with surface evaporation
c. Volume evaporation
d. Formation of an optically thick plume

e. Plasma absorption in the plume

f. Optical breakdown (in transparent insulators)

The separation of these regimes according to the principal determining factors (i.e., laser irradiance, I_0, and the solid optical absorption coefficient, α) are shown in Figure 3A.2. The three different thresholds—here volatilization threshold, I_0^{volat}, plasma ignition threshold, I_0^{plasm}, and optical breakdown threshold, I_0^{break}—are marked by dashed vertical lines. Although their values are well defined, variations can be expected in a given experiment according to the choice of laser or target material.

In an earlier study we dealt with the transition from normal absorption of the laser-generated plume to plasma absorption characterized by 10^8–10^9 W/cm^2 threshold irradiance (Vertes et al., 1989a). For this high-irradiance transition between regimes d and e, the threshold was established on the basis of investigating normal absorption vs. plasma absorption.

Matrix-assisted laser desorption is a much milder process typically requiring about 10^6 W/cm^2 irradiance and low-melting-point or low-sublimation-temperature material. Recently, it has been shown by elaborate irradiance threshold measurements that the underlying process is a collective effect, similar in principle to phase transitions (Ens et al., 1991). Furthermore, threshold irradiance values change little by changing the mass of the guest mole-

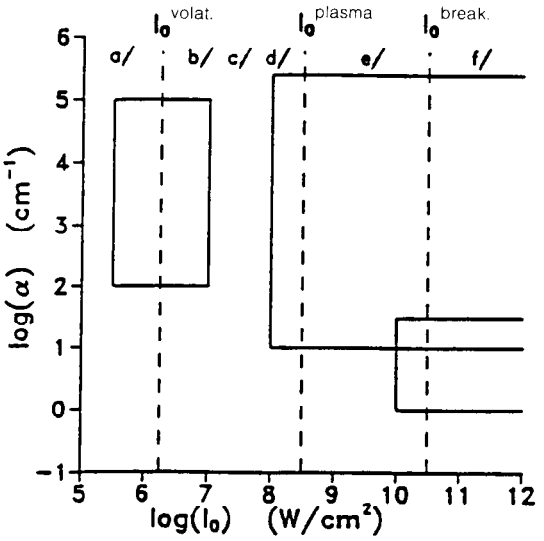

Figure 3A.2. Different regimes of laser solid interaction are roughly divided according to laser irradiance and optical absorption coefficient. From Vertes (1991b) with permission of San Francisco Press Inc. See explanation in text.

cules over an order of magnitude (Hedin et al., 1991). Therefore, we assume that the threshold of our concern marks the transition between regimes a and b or between processes a and c. To estimate the required irradiance we set the following condition: in order to reach volatilization due to laser heating the elevated surface temperature, T_{surf}, must exceed the melting or sublimation temperature of the matrix, T_{subl}:

$$T_{surf} \geq T_{subl} \tag{4}$$

The rise of surface temperature, $\Delta T_{surf}(t)$, at time t under the influence of a uniform penetrating light source with I_0 irradiance is (von Allmen, 1987, p. 55):

$$\Delta T_{surf}(t) = \frac{I_0}{K}\left\{\frac{\delta}{\pi^{1/2}} - \frac{1}{\alpha}\left[1 - \exp\left(\frac{\alpha\delta}{2}\right)^2 \operatorname{erfc}\left(\frac{\alpha\delta}{2}\right)\right]\right\} \tag{5}$$

Table 3A.1. Melting Temperatures and Wavelengths and Molar Extinction Coefficients of UV Absorption Maxima for Most Successful Matrices Used in Laser Desorption of Peptides and Proteins

Laser Desorption Matrix	T_m (°C)	λ_{max} (nm)	ε_{max} (L/mol·cm)
Nicotinic acid (3-pyridinecarboxilic acid)	236	262 217	2750 8610
Pyrazinoic acid (2-pyrazinecarboxilic acid)	225	267 208	7820 7960
Vanillic acid (4-hydroxy-3-methoxybenzoic acid)	214	259 217	11900 22900
Sinapinic acid (*trans*-3,5-dimethoxy-4-hydroxy-cinnamic acid)	192	240 320	10000 15849
Caffeic acid (*trans*-3,4-dihydroxycinnamic acid)	225	324 297 235	n.a.[a]
Ferrulic acid (*trans*-4-hydroxy-3-methoxy-cinnamic acid)	171	320 235	n.a.
2,5-Dihydroxybenzoic acid	205	335 237	n.a.

Source: From Grasselli and Ritchey (1975).
[a]n.a. = not available.

where $\delta = 2(\kappa t)^{1/2}$ and the thermal diffusivity $\kappa = KV_M/c_p$; here K, V_M, and c_p are the thermal conductivity, the molar volume, and the specific heat of the material, respectively. Although analytical formulas are shown to overestimate the temperature jump in pulsed surface heating, at the irradiances of our concern ($< 5 \times 10^7$ W/cm^2) the error is negligible (Philippoz et al., 1989).

If we substitute the values for material parameters of nicotinic acid ($\alpha_{265} = 4 \times 10^4$ cm^{-1}; $c_p = 150$ J/mol·K; $V_M = 83.5$ cm^3/mol; $K = 2 \times 10^{-3}$ W/cm·K), the surface temperature rise is $\Delta T_{surf}(t) = 202$ K by the end of a frequency-quadrupoled Nd:YAG laser pulse ($t = 10$ ns; $I_0 = 10^6$ W/cm^2). This value, if superimposed on room temperature, compares extremely well with the sublimation temperature of the matrix $T_{subl} = 236$ °C. Detailed investigations show the threshold irradiance of ion generation with MALD for both the nicotinic acid matrix (Beavis and Chait, 1989a) and the sinapinic acid matrix (Ens et al., 1991) to be around 10^6 W/cm^2. The most successful matrices, their melting points, and light absorption characteristics are listed in Table 3A.1. Other quantities influencing Eq. (5), such as K, V_M, and c_p, differ little for these materials. Based on these data, Eq. (5) can be evaluated for the listed matrices. The calculated threshold irradiances show insignificant variation in accordance with experimental observations.

3A.4. MATRIX-ASSISTED LASER DESORPTION

Matrix-assisted laser desorption (MALD) as a soft volatilization and ionization technique was introduced a few years ago (Tanaka et al., 1988; Karas and Hillenkamp, 1988). Since then it has acquired the reputation of being a strong candidate for the analysis of high-molecular-weight biopolymers. MALD stayed in competition with electrospray ionization for the availability of a similar mass range and for their comparable detection limits. In other respects, e.g., the problem of interferences and coupling to separation techniques, they are considered to be complementary methods. However, in the atmosphere of excitement caused by the vast array of potential new applications, not too much attention has been paid to answer basic questions concerning the mechanism of the volatilization and ionization phenomena.

In laser desorption experiments the sample should have a high absorption coefficient at the laser wavelength. For commonly used ultraviolet (UV) lasers, this condition is not met for a large number of important biomolecules. Early on, the idea of mixing these samples with a good absorber came as a possible enhancement method (Karas et al., 1987). Indeed, resonantly absorbing substances exhibited about an order of magnitude lower threshold irradiances than the analytes themselves. The lower the irradiance is, the softer the ionization method can be considered.

Based on this observation, the MALD method was introduced, essentially as a special sample preparation technique. In the first version of the experiment a dilute solution of the analyte ($\sim 10^{-5}$ M) was mixed with an equal amount of a 5×10^{-2} M aqueous solution of nicotinic acid. Solutions of the large (guest) molecules and of the matrix (host) material were mixed, providing 1:1000 to 1:10,000 molar ratios. A droplet of this mixture was air-dried on a metallic substrate and introduced into the mass spectrometer. Moderate irradiance (10^6–10^7 W/cm^2) frequency-quadrupoled Nd:YAG laser pulses (266 nm, 10 ns) were used to desorb and ionize the sample. The generated ions were typically analyzed by a time-of-flight mass spectrometer. The astonishing finding was that extremely large molecules (molecular weight exceeding 100,000 Da) could be transferred to the gas phase and ionized by this method.

Achieving softer ionization conditions for a broader class of materials was a remarkable advance in itself. Further developments came with the

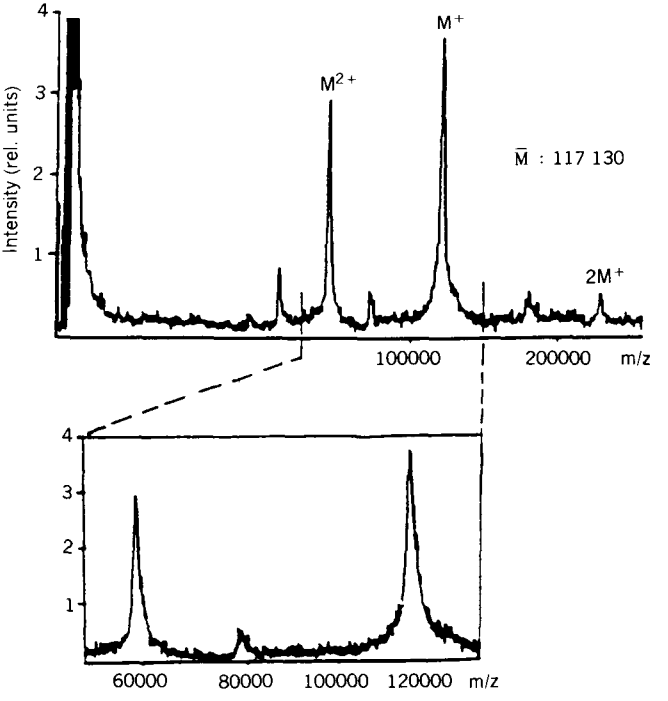

Figure 3A.3. High-mass region MALD mass spectrum of β-D-galactosidase enzyme. Signal averaging improved the signal-to-noise ratio (30 shots). From Karas et al. (1989b) with permission of VCH Verlagsgesellschaft mbH.

introduction of about 20 keV postacceleration at the end of the flight tube. The purpose of this modification was to increase the detection sensitivity for large mass ions. These particles otherwise hit the conversion dynode of the electron multiplier detector with relatively low velocity, resulting in poor conversion. Laser desorption of large ($m/z > 10{,}000$) (Karas and Hillenkamp, 1988) and very large ($m/z > 100{,}000$) (Tanaka et al., 1988; Karas et al., 1989a) ions generated great interest among mass spectroscopists who had been struggling with the volatilization problem for more than a decade.

Owing to the extended mass range, several important classes of molecules (proteins, certain polymers) became available for mass spectrometric analysis and investigation. A typical β-D-galactosidase MALD spectrum is shown in Figure 3A.3. Better preparation procedures and the introduction of new matrices yielded even higher upper mass limits, reaching $m/z \approx 250{,}000$ Da (Karas et al., 1989b). These findings had a considerable impact on the pace of laser desorption investigations. In the 1988–1992 period the number of related articles showed exponential growth as a consequence of the discovery of MALD.

A growing number of groups joined the investigation (Beavis and Chait, 1989a; Nelson et al., 1989; Salehpour et al., 1989; Ens et al., 1990; Frey and Holle, 1990; Hettich and Buchanan, 1990; Nuwaysir and Wilkins, 1990; Spengler and Cotter, 1990; Vertes et al., 1990b; Zhao et al., 1990a). Detection limits ranging from 5 pmol to 50 fmol and mass accuracy of about 0.1% were established (Karas et al., 1989c). Both characteristics, however, showed strong sample dependence. Beavis and Chait (1989b) introduced cinnamic acid derivatives as new matrix materials showing similar or superior features to nicotinic acid. Negative ion spectra of proteins were also observed (Beavis and Chait 1989a; Salehpour et al., 1989). High-mass glycoproteins and hydrophobic proteins not accessible to plasma desorption mass spectrometry showed encouraging response in MALD experiments (Salehpour et al., 1990).

Mass accuracy of the MALD method was squeezed to $\pm 0.01\%$ by using internal calibration of the mass scale (Beavis and Chait, 1990a). In most cases, the required sample amount (0.5–1.0 μL of sample solution containing several picomoles or several hundred femtomoles of analyte) compared favorably with the sample requirements of other mass spectroscopic techniques.

Frequency-tripled Nd:YAG laser ($\lambda = 355$ nm) was successfully tried to demonstrate that MALD is feasible with more affordable nitrogen lasers ($\lambda = 337$ nm) (Beavis and Chait, 1989c). Recently, possibilities have been broadened even further by the experiments on MALD using infrared (IR) radiation of Q-switched Er:YAG laser ($\lambda = 2.94\ \mu$m) (Overberg et al., 1990) and of CO_2 laser ($\lambda = 10.6\ \mu$m) (Hillenkamp, 1990).

Some early efforts were directed toward broadening the range of applicable matrices and laser wavelengths and resulted in a rough outline of required

matrix material properties (Beavis and Chait, 1990c). A promising candidate for a successful matrix should exhibit the following features:

a. Strong light absorption at the laser wavelength
b. Low volatilization temperature (volatilization shall take place preferably in the form of sublimation)
c. Common solvent with the analyte
d. Ability to separate and surround the large molecules in a solid solution without forming covalent bonds

With these principles in mind several groups set out to search for appropriate and better matrices. In a thorough study Beavis and Chait (1990c) tested about 50 different matrix materials. When UV lasers were used the best results in peptide volatilization and ionization could be obtained by applying nicotinic acid, 2,5-dihydroxybenzoic acid, pyrazynoic acid, vanillic acid, ferrulic acid, sinapinic acid, caffeic acid, and certain other cinnamic acid derivatives. The important optical and thermal properties of some UV matrices are listed in Table 3A.1. Nitrobenzyl alcohol on fibrous paper substrate turned out to be a useful matrix as well (Zhao et al., 1990b). In addition to the matrices used in the UV experiments carboxylic acids, glycerol, urea and tris buffer proved also to be applicable in the IR experiments. Low analyte specificity and moderate volatility in the vacuum system complemented the list of desirable features expected from prospective matrices.

Experiments aimed at further elucidating the physical background of the MALD phenomena were launched in several laboratories. Initial kinetic energy distributions of MALD-generated ions were measured utilizing pulsed ion extraction in a Wiley–McLaren-type time-of-flight instrument (Spengler and Cotter, 1990). Departing ion energies showed about 1 eV mean value. The question of substrate participation was analyzed in a study where laser and ion optics were situated on opposite sides of suspended sample crystals (Vertes et al., 1990b). Successful matrix-assisted experiments on various low-mass peptides supported the idea of negligible substrate participation with strongly absorbing matrices.

Several groups were able to establish laser irradiance thresholds of ion generation (e.g., see Hedin et al., 1991; Ens et al., 1990). Threshold phenomena had been reported many times earlier in the general context of laser ionization. Although the absolute numbers for irradiance varied from study to study or even from sample to sample, the values were generally somewhere around several times 10^6 W/cm^2. These uncertainties were attributed to poorly defined light intensity measurements and to uncontrolled variations in sample morphology. Ens et al. (1990) used single ion counting to determine the irradiance threshold of insulin ion generation and the irradiance dependence

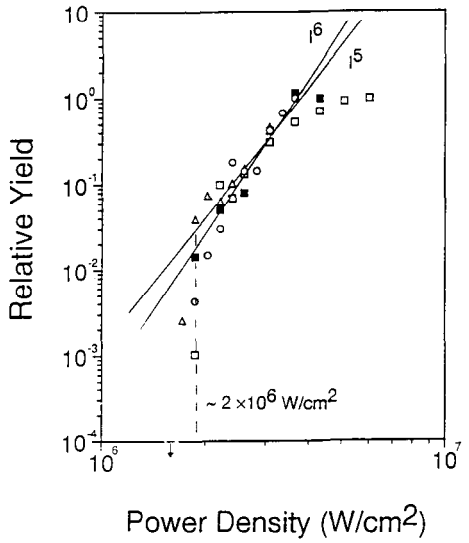

Figure 3A.4. Irradiance dependence of the insulin molecular ion yield clearly exhibits threshold behavior. From Ens et al. (1990) with permission of John Wiley & Sons, Ltd. The various symbols correspond to different detector openings.

of ion yield (see Figure 3A.4). With the analysis of pulse height distributions it also was inferred that MALD is the result of collective processes. In a different experiment it was shown that mass spectrometry is not the only method to separate and detect the large molecules (Williams, 1990).

Velocity distributions were measured for high-mass polypeptide molecular ions (Beavis and Chait, 1991b) and for neutral molecules of gramicidin S (Huth-Fehre and Becker, 1991) generated by MALD. There were several important observations in these studies. The polypeptide molecular ions showed similar *velocity* distributions, exhibiting 750 m/s average velocity independent of molecular mass in the 1000–15,600 Da range. This result was interpreted as an indication of jet-expansion-type processes during the desorption (Beavis and Chait, 1991b). Velocity distribution measurements on neutral molecules of ferrulic acid matrix and gramicidin S, a 1141.5 Da peptide, indicated common velocity maximum between 300 and 400 m/s (Huth-Fehre and Becker, 1991). This value is in good agreement with the drift velocities established by the cool plume model (see Section 3A.6.2, below). It is also remarkable that the matrix and the guest molecules showed very similar velocity distributions.

Detection mechanisms of large molecules were investigated in order to improve detection efficiency (Spengler et al., 1990c; Kaufmann et al., 1991). With increasing molecular weight of the 5–40 keV primary ions, secondary

electron emission at the conversion dynode was found to be diminishing and to give rise to the generation of small secondary ions. Tandem time-of-flight measurements revealed the nature of these secondary ions. The negative secondary ion spectra consisted of H^-, C_2H^-, and $C_2H_2^-$ ions, whereas the positive secondary ions were identified as H^+, Na^+, K^+, and ions at $m/z = 28$, 41, 43, 45, 73 and minor components up to $m/z = 326$ (Kaufmann et al., 1992). The formation of these secondary ions was attributed to sputtering of surface contaminants rather than collision-induced dissociation of the primary ions.

Preliminary results were reported on the metastable decay of MALD-generated ions: 354.5 nm laser desorption of insulin molecules resulted in molecular ions decaying in the field-free flight tube, losing probably a relatively small neutral entity (Beavis and Chait, 1991a). Beavis and Chait also concluded that metastable decay is an indication of high internal (vibrational) temperatures of the desorbed ions. Metastable decay of peptide and protein ions in MALD was also observed in a time-of-flight instrument with an ion reflector (Spengler et al., 1991; Spengler and Kaufmann, 1992). The decay channels were sample specific but generally included the loss of ammonia and segments of amino acid side chains. This postsource decay showed potential to extract structural information on peptides and proteins.

Desorbed neutrals and molecular ions were investigated using tunable UV laser light for desorption, supersonic jet cooling, and resonance-enhanced multiphoton ionization (REMPI) (Frey and Holle, 1990). It is instructive to compare the effect of matrix assistance and supersonic cooling on the fragmentation patterns. Without cooling and without matrix no molecular ion signals were observed for gramicidin D (MW = 1881), whereas the introduction of either jet cooling or matrix assistance alone was sufficient to suppress the fragmentation. Preliminary estimates of neutral velocity distributions indicate about 300 K translational temperature, independent of laser wavelength ($\lambda = 10.6\,\mu m$ or 266 nm).

Pilot experiments to utilize MALD in Fourier transform mass spectrometers (FTMS) have been described (Hettich and Buchanan, 1990). Low-mass ions ($m/z < 2000$) exhibited strong matrix enhancement under FTMS conditions, but efforts to detect molecular ions in the higher mass region were unsuccessful. The origin of this deficiency was linked to the detection limitations of the FTMS instrument. Another attempt to combine MALD with FTMS concluded that the nicotinic acid matrix material sublimed from the probe tip within 15 min under the usual vacuum of FTMS measurements (10^{-8} torr) (Nuwaysir and Wilkins, 1990). Possible alternatives for matrix material were tested, with encouraging results in the case of sinapinic acid and sucrose. High-mass capabilities of MALD-FTMS have been demonstrated only recently by Castoro et al. (1992). With proper adjustment of the

ion source they were able to detect ions with masses as high as 34,000 Da. Some spectra showed much higher mass resolution than those obtained by time-of-flight instruments.

Recently, a different scheme of laser volatilization has been introduced (Nelson et al., 1989; Becker et al., 1990). Thin films of the aqueous analyte solution were frozen onto cooled metal probe tips. The laser radiation ablated the ice film. The volatilized material was either collected on a solid surface and subsequently analyzed using gel electrophoresis or directly analyzed by time-of-flight mass analysis with or without postionization. Electrophoresis results on DNA digest showed very-high-mass particles ($m/z \approx 6$ MDa) in the plume, whereas TOF detection revealed $m/z \approx 18{,}500$ ions (Nelson et al., 1990). These results were rationalized in terms of sudden heating of the metal surface followed by fast heat transfer to the ice layer and by explosive boiling (Nelson and Williams, 1990).

3A.5. MALD IN THE ANALYSIS OF BIOLOGICAL MOLECULES

Applications of MALD-MS are just beginning to mushroom. The most important achievements are expected in areas where the unique features of the method can be utilized. The unparalleled mass accuracy in the high-mass region have even made it possible to revise the calibration curves of certain commercial gel electrophoresis molecular weight marker kits (Kratzin et al., 1989).

3A.5.1. Peptides and Polypeptides

Although many of the peptides can be readily analyzed by fast atom bombardment (FAB), there are special classes of these materials where MALD has demonstrated a competitive advantage. Most significantly, ion production from high-molecular-weight polypeptides by MALD does not show the cutoff around 5000 Da quite customary in the case of FAB measurements. Bovine trypsin inhibitor (6500 Da), melittin (2847 Da), and Met-Lys bradykinin (1320 Da) were studied with MALD to assign correct molecular weights to molecular weight marker kits (Kratzin et al., 1989).

An important feature of MALD is its relatively uniform sensitivity to different peptides. FAB tends to provide unstable or low ion currents for hydrophilic peptides, whereas MALD spectra show no deterioration for this important class of compounds. Two neuropeptides (substance P and bombesin), six analogues of melanocyte-stimulating hormone core, and collagenase enzyme substrates were investigated using transmission geometry MALD. Strong molecular ion peaks were present in the positive ion spectra, indepen-

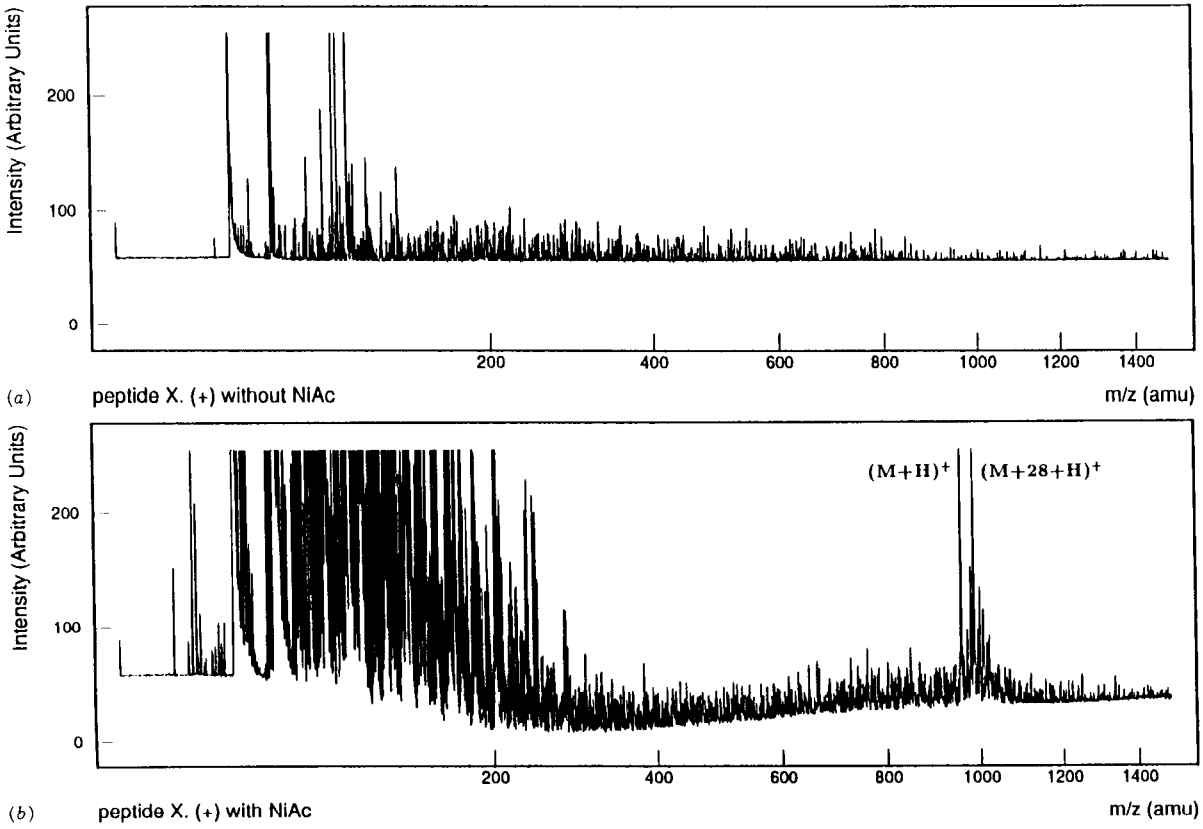

Figure 3A.5. Single shot laser desorption spectra of a melanocyte-stimulating hormone core analogue peptide (H-Nle-Glu-His-(D)Phe-Arg-Trp-Gly-OCH_3)·3HCl in transmission geometry: (a) without and (b) with matrix assistance. No peptide-specific ions are observed without matrix. The matrix-assisted method shows dramatic enhancement of the molecular ion signal. From Vertes et al. (1990b) courtesy of John Wiley & Sons Ltd.

dent of the chemical nature of the peptide (Vertes et al., 1990b). In Figure 3A.5 the dramatic enhancing effect of the matrix is demonstrated for (H-Nle-Glu-His-(D)Phe-Arg-Trp-Gly-OCH_3)·3HCl.

MALD shows detection limits in the femtomol and subfemtomole range for peptides (Strobel et al., 1991). This is clearly an asset in many areas of biochemical research (neuropeptides, etc.) where often only minute traces of the analyte are available.

A combination of enzymatic digestion and MALD can contribute to protein sequence determination. This technique is based on the capability of MALD to produce interference-free spectra of complex mixtures. Digestion of the protein by the appropriate enzyme provides a mixture of peptide fragments that can be analyzed at different stages of degradation by MALD (Schaer et al., 1991a,b). In another study, peptide sequencing is envisioned utilizing metastable decay in the field-free region of a reflectron-type time-of-flight spectrometer (Spengler et al., 1992).

3A.5.2. Proteins

Most of the measurements involving MALD have been carried out on proteins. From the time of the effect's discovery, most of the initial exploratory-type experiments have used protein samples. Here, however, we shall only focus on protein studies emphasizing applications.

Protein molecular mass determinations are particularly straightforward with MALD. The most intensive peaks in the high-mass region of the spectra are often related to the protonated molecules. Doubly and multiply charged molecular ions, as well as cluster ions, are also formed under certain conditions. The purity and molecular mass of proteins were investigated early on in several laboratories (Gabius et al., 1989; Karas et al., 1989c; Salehpour et al., 1989; Beavis and Chait, 1990d).

It is very rare to observe fragment ions using the matrix-assisted technique. This feature makes it easy to find the molecular mass of proteins. To recover the primary structure, however, knowledge of fragmentation patterns is necessary. As we mentioned earlier, several groups suggested getting around this problem by utilizing enzymatic digestion (Schaer et al., 1991b; Juhasz et al., 1992; Chait et al., 1992). Both digestion with carboxypeptidases Y and B and tryptic digestion are used in combination with MALD. By calculating the mass differences between peptides successively degraded by carboxypeptidase, it is possible to identify the released amino acids. With tryptic digestion, an amino acid sequence can be confirmed within minutes, providing unprecedented ease and rapidity of analysis.

Further development is expected in enhancing sequencing capabilities by MALD. One option is to observe metastable decay of laser-desorbed ions.

These processes take place in the field-free drift region of the time-of-flight mass spectrometer. In a preliminary study several useful fragmentation pathways of relatively small peptides were observed (Spengler et al., 1992). Another possible way to increase fragmentation is to use less effective matrices or matrix mixtures (Wilkins et al., 1992).

MALD also is useful to detect the presence or absence of certain functional groups on large proteins. Because of its superior mass accuracy MALD is

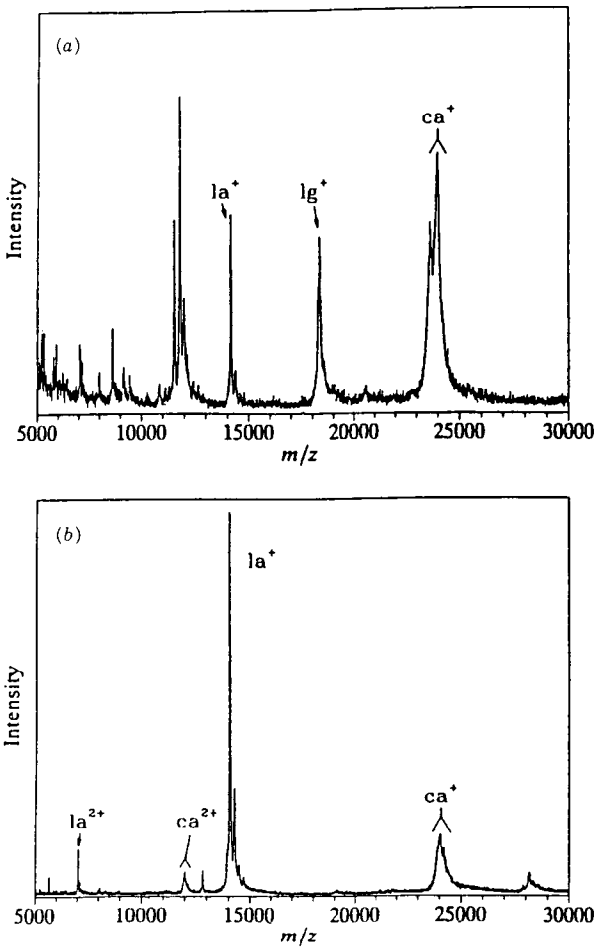

Figure 3A.6. Mass spectra of complex mixtures obtained from commercial bovine milk (a) and human breast milk (b). Several protein peaks are labeled [lactalbumin (la), lactoglobulin (lg), and casein (ca)], with the protonation states of the ions also indicated. From Beavis and Chait (1990d) with permission of the authors.

able to distinguish between untreated monoclonal antibodies and their derivatives conjugated with chelators and drugs (Siegel et al., 1991). Similarly, metal binding properties of protein surfaces can be studied (Yip and Huthchens, 1992). Mass accuracy for very large protein molecules ($\sim$ 150,000 Da) is around $\pm 0.1\%$. Therefore, the presence of conjugated units is detected if their mass exceeds 150 Da. In the case of smaller protein substrates the mass accuracy can reach 0.01%, providing increased potential for functional group identification.

Mixtures of proteins are also readily analyzed by MALD. Proteins produce spectra even in complex mixtures of organic and inorganic constituents such as unpurified biological fluids. This feature was emphasized in an experiment where the mass spectra of commercial bovine milk and human breast milk were taken (Beavis and Chait, 1990b,d) (see Figure 3A.6). Physiological salt concentrations—usually prohibitive for other MS methods—are not detrimental to MALD spectra (Karas et al., 1990b). A comparative study of MALD and electrospray MS showed clear advantages in favor of the MALD technique, particularly for mixtures of more than two components (Allen et al., 1991). Off-line coupling of MALD with separation techniques such as high-performance liquid chromatography (HPLC), thin-layer chromatography (TLC), and gel electrophoresis further enhances the possibilities of mixture analysis.

One of the most promising applications of MALD is related to identifying protein expression errors and to investigating posttranslational modifications such as glycosylation, phosphorylation, sulfation, proteolytic processing, and disulfide bond formation among others. The method is based on comparing the molecular weight of the protein as measured by MALD to its value calculated from the related DNA sequence, or to its value without modification. The difference between these values can reveal protein expression errors (Keough et al., 1992) or even the nature of a small blocking group (Hillenkamp et al., 1991). A number of possible posttranslational modifications and the associated mass change are listed in Table 3A.2. Measuring the mass and determining the sequence of a protein produced by translation can also help in confirming the sequence of the original DNA.

Monitoring and quality control of protein synthesis and identification of by-products are also among the demonstrated capabilities of MALD (Boernsen et al., 1991). Comparison of reversed-phase HPLC, tricine–sodium dodecyl sulfate–poly(acrylamide) gel electrophoresis (SDS-PAGE) and MALD in the detection and identification of impurities in commercial β-galactosidase (MW $\sim$ 100,000 Da) showed unambiguous advantages of MALD. Both other methods require more sample preparation and longer analysis time, and also provide less accurate mass information on the unknown species. In purification during synthetic peptide production and in

Table 3A.2. Posttranslational Modifications of Proteins and Resulting Mass Changes

Posttranslational Modification	Mass Change (Da)
Acetylation	42.04
Biotinylation (amide bond to lysine)	226.29
Carboxylation of Asp and Glu	44.01
C-terminal amide formed from Gly	−0.98
Cysteinylation	119.14
Deamidation of Asn and Gln	0.98
Deoxyhexoses (Fuc)	146.14
Disulfide bond formation	−2.02
Farnesylation	204.36
Formylation	28.01
Hexosamines (GlcN, GalN)	161.16
Hexoses (Glc, Gal, Man)	162.14
Hydroxylation	16.00
Lipoic acid (amide bond to lysine)	188.30
Methylation	14.03
Myristoylation	210.36
N-Acetylhexosamines (GlcNAc, GalNAc)	203.19
Oxidation of Met	16.00
Palmitoylation	238.41
Pentoses (Xyl, Ara)	132.12
Phosphorylation	79.98
Proteolysis of a single peptide bond	18.02
Pyridoxal phosphate (Schiff base formed to lysine)	231.14
Pyroglutamic acid formed from Gln	−17.03
Sialic acid (NeuNAc)	291.26
Stearoylation	266.47
Sulfation	80.06

Source: From Finnigan MAT (1991).

protein separation from biological products, HPLC is the method of choice. Therefore, it is not surprising that when used to assess the homogeneity of the purified product HPLC is often not able to resolve components which co-purify with the compound of interest. MALD, based on a completely different physical principle, is usually successful in these hard-to-handle situations.

Quantitation of proteins with MALD is under investigation too (Nelson

et al., 1992). Preliminary results show linear response over 1 decade concentration range, using internal protein standards and the standard addition method. The estimated error of concentration determination is 10–20%.

3A.5.3. Nucleotides

There is limited experience with MALD of nucleotides. Preliminary studies show that volatilization of deoxyribonucleic acids (DNA) is possible both from frozen aqueous solutions (Nelson et al., 1989) and from rhodamine 6G dye matrix (Romano and Levis, 1991). In the first study the excimer pumped dye laser operated at 581 nm, where the DNA and the water matrix are transparent. The laser energy was therefore deposited into the copper substrate. In the second investigation, a frequency-doubled Nd:YAG laser was used at 532 nm, very close to the absorption maximum of rhodamine 6G (526 nm). After collecting the ablated material on a target both groups used PAGE for separation and autoradiography for detection. When the autoradiograms of the ablated and collected material are compared to the band distributions from the starting digest, it appears plausible that DNA molecules up to 410 kDa (622 base pairs) survived the vaporization intact or with very little fragmentation.

Mass spectrometric detection of the volatilized species is much more difficult. Molecular ions of double-stranded oligomeric nucleic acids were produced from frozen aqueous matrix only up to masses ~ 18,500 Da (Nelson et al., 1990). Smaller oligonucleotides in the mass range below 2000 Da

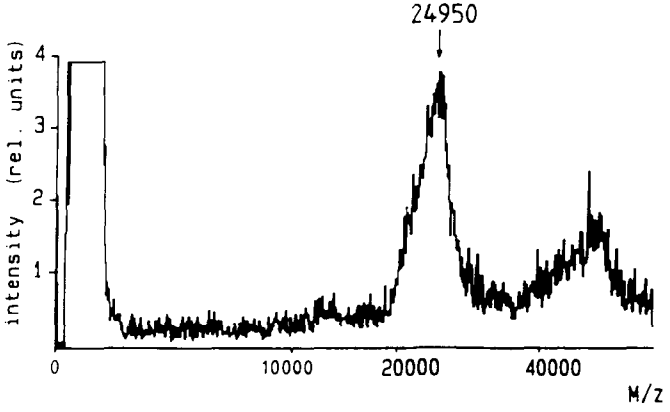

Figure 3A.7. Laser desorption–ionization mass spectrum of yeast t-RNA of molecular weight 24,952 Da; 0.1 $\mu g/\mu L$ aqueous solution mixed with 5×10^{-2} mol/L nicotinic acid. Average of 20 single spectra. From Hillenkamp et al. (1990) courtesy of Elsevier Science Publishers B.V.

desorbed from nicotinic acid matrix also exhibited significant molecular ion signals (Spengler et al., 1990b). Yeast t-RNA of mass 24,952 Da was desorbed using 266 nm laser radiation (Hillenkamp et al., 1990). So far, this is among the largest nucleotide ions observed in a mass spectrometer. In Figure 3A.7 one can notice the corresponding broad and asymmetric molecular ion peak. The lower edge tailing of this peak is believed to be the consequence of gradual nucleobase cleavage from the RNA ion. Indeed, the related nucleobase ion signals were detected in the low-mass region of the spectrum.

Difficulties with mass spectrometric detection of intact nucleotide ions can be attributed to their strong UV absorption and to their reduced ability to accommodate positive charge. To overcome these obstacles future experiments will need to focus on finding matrix-laser combinations that ensure selective energy deposition into the matrix and utilize negative ions and neutrals for increased detection efficiency.

3A.5.4. Carbohydrates

Application of matrices for carbohydrate analysis provides less impressive spectrum enhancement over conventional techniques than it does for proteins. The standard method of measuring oligosaccharides by mass spectrometry is derivatization followed by FAB analysis. Permethylation or peracetylation of carbohydrates often improves the sensitivity of FAB analysis by about an order of magnitude. The accessible molecular weight range for this method, however, does not exceed 3500 Da.

FAB or liquid secondary ion mass spectrometry (SIMS) determination of carbohydrates, especially in their underivatized form, also is hindered by low ion yields. To overcome this difficulty matrix assistance was introduced long before the discovery of MALD (Harada et al., 1982): α- and γ-cyclodextrin and some smaller oligosaccharides were measured using diethanolamine matrix to produce abundant amine adduct ion peaks. Other FAB matrices and matrix mixtures were also assessed (Voyksner et al., 1989). With this method quasi-molecular ions up to 3700 Da are detected in the positive ion FAB spectra of native oligosaccharides.

In some cases direct laser desorption offers a practical alternative. Extensive fragmentation has recently been observed in IR laser desorption of neutral oligosaccharides (Martin et al., 1989; Spengler et al., 1990a). Fragmentation patterns are useful for structure elucidation and provide complementary information to FAB experiments. The major fragmentation pathway has been identified as a retro-aldol-type pericyclic hydrogen rearrangement leading to fragmentation of the sugar ring (Spengler et al., 1990a). The presence of this process depends on the opening of the hemiacetal saccharide ring to the linear saccharide form. Cyclic acetals usually do not exhibit this

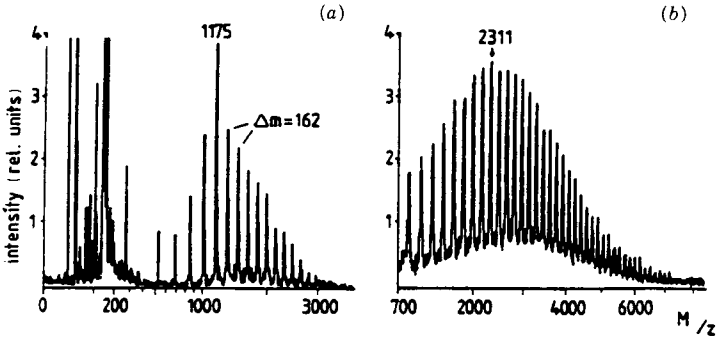

Figure 3A.8. Matrix LDI spectrum of maltodextrins (a) and dextrans (b). The various oligoglucan species differ in mass by 162 Da as indicated in the figure. *Conditions:* matrix, dihydroxybenzoic acid; sample, 100 ng (a), 200 ng (b). The spectra are averages of 20 (a) and 60 (b) single spectra. From Stahl et al. (1991) with permission of the American Chemical Society.

reaction; therefore the presence of the corresponding derivatives can be detected.

MALD analysis of glucans, oligofructans, mannose-containing oligosaccharides (Stahl et al., 1991), dextran hydrolyzates, high-mannose oligosaccharides (Mock et al., 1991), and cyclodextrins (Boernsen et al., 1990) has been shown to have significant advantages. Among them are the high throughput of the measurement and the direct information on molecular masses. Typical analysis time is around 5–15 min, which compares favorably with the duration of gel filtration and HPLC determinations. Mass spectrum evaluation is made simple by the lack of fragmentation and by the dominance of alkalinated quasi-molecular ions. Typical spectra of maltodextrins and dextrans are displayed in Figure 3A.8. Carbohydrate-related ions can be observed up to 7000 Da exhibiting clear improvement over earlier techniques. Another advantage of MALD is the capability of measuring complex carbohydrate mixtures. Figure 3A.8b shows as many as 39 dextran components. Furthermore, as we discussed earlier, the technique is relatively insensitive to the presence of inorganic salts. These features make it possible to simplify sample preparation (for example, no desalting is needed) and save some of the separation steps as well.

3A.5.5. Other Compounds

An obvious and very important extension of the MALD technique would be its application to polymers of industrial origin. This idea was already present in one of the first publications describing MALD (Tanaka et al., 1988). Poly(propylene glycol) with an average molecular weight of 4 kDa

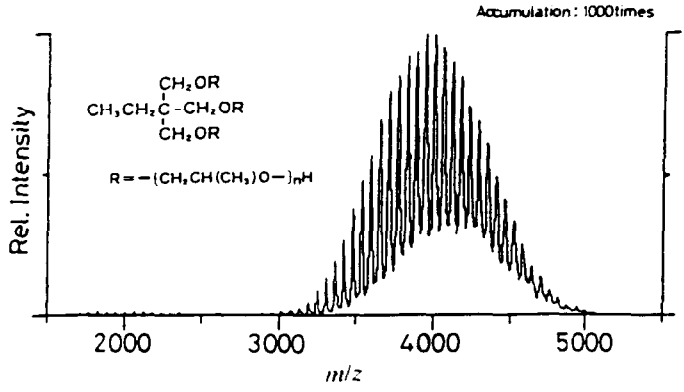

Figure 3A.9. Laser ionization mass spectrum of poly(propylene glycol). Average molecular weight is 4 kDa (PPG4K). From Tanaka et al. (1988) courtesy of Heyden & Sons, Ltd.

(PPG4K) and the 20 kDa fraction of poly(ethylene glycol) (PEG20K) were investigated. The matrix was glycerol suspension of ultrafine cobalt powder (300 Å diameter particles). The PPG4K spectrum is shown in Figure 3A.9. More recent investigations include the measurement of PEG 8K and PEG10K fractions using a sinapinic acid matrix and Fourier transform mass spectrometry (FTMS) detection (Castoro et al., 1992).

The larger and more important group of polymers showing no solubility in water has not yet been measured successfully with MALD. There are several ways to address this task. One possibility is to search for matrices showing good solubility in the organic solvents of these polymers and low sublimation temperatures. Some compounds exhibiting these features are polyaromatic hydrocarbons (PAH). These compounds show strong light absorption at the wavelength of the frequency-quadrupled Nd:YAG laser (266 nm) and readily form radical cations even at very low irradiances. Another approach could be to enhance ion generation. This can be accomplished by using strong ionizing agents in the matrix or by the introduction of a second ionizing laser pulse across the plume.

Highly thermolabile compounds constitute another class of materials that can benefit from the gentle ionization of MALD. An interesting example is vitamin B_{12}. Vitamin B_{12} is itself a strong absorber at 266 nm; therefore its quasi-molecular ions cannot be observed without a matrix. Introduction of nicotinic acid matrix, however, yields a strong $[M+H—CN]^+$ ($m/z = 1239$) ion signal at threshold irradiance (Karas et al., 1987). Increasing the laser irradiance leads to partial fragmentation. At 10 times the threshold irradiance the degree of fragmentation is comparable to the situation without a matrix. Aryltriphenylphosphonium halides represent a group of compounds with

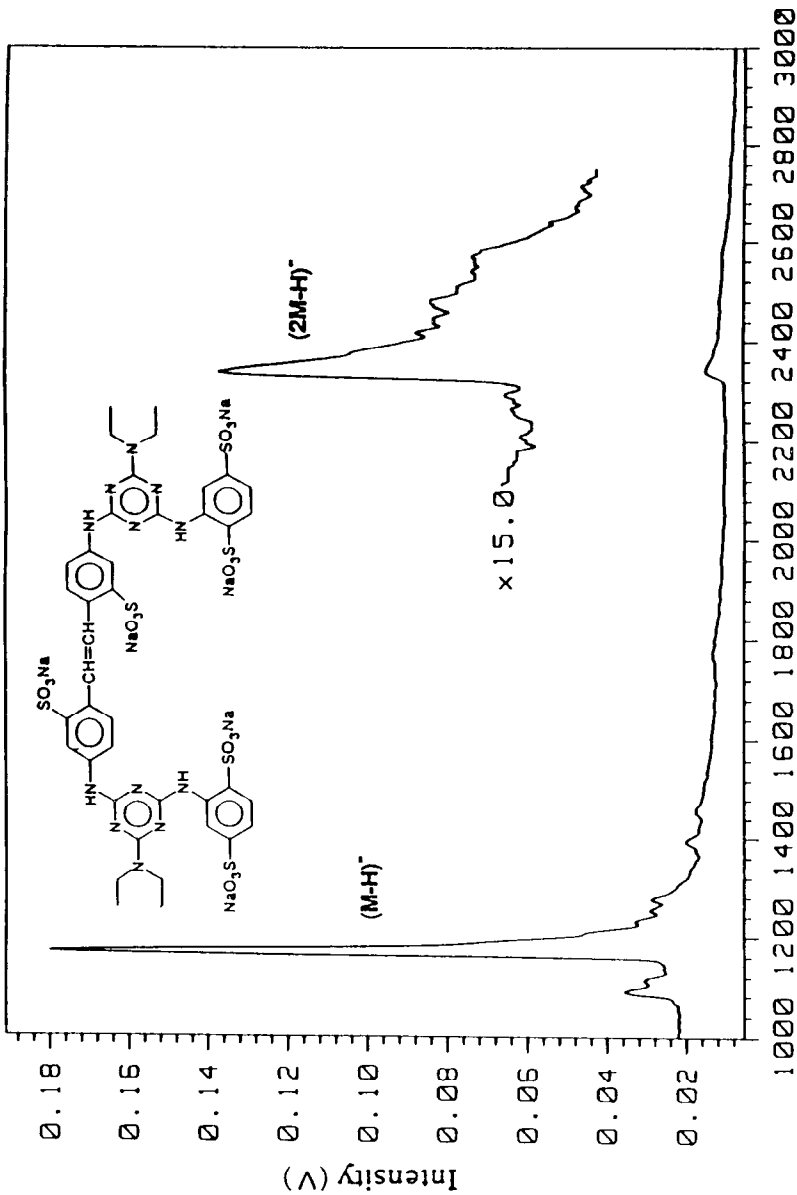

Figure 3A.10. Negative MALD spectrum of a sulfonic acid. Sixteen shots were averaged. From Boernsen et al. (1990).

extreme thermal instability. 1-Naphthylmethyltriphenylphosphonium chloride, for example, can decompose under the slightest thermal load and provide $m/z = 402$ cations. In the presence of nicotinic acid matrix, however, intact molecular ions can be observed (Claereboudt et al., 1991). Sulfonic acids also were measured in the negative ion mode using an Nd:YAG pumped dye laser at 330 nm and sinapinic acid matrix (Boernsen et al., 1990). The molecular ion and the dimer ion peaks at $m/z = 1173.8$ and $m/z = 2350.9$, respectively, are shown in Figure 3A.10. At this point we can conclude that compounds very different in chemical nature are amenable to analysis with MALD.

Rapid development in the diversification of MALD applications is expected in the near future, although the inertia of the standard biochemical approach is immense. Molecular weight determination of large biomolecules is routinely done as part of the gel electrophoresis separation step. It is difficult to compete in price and in ease of operation with the conventional method, especially since the introduction of precast gels has considerably shortened the analysis time. MALD will have to offer substantial superiority in certain features in order to get widespread recognition. The price of the instrumentation will still be prohibitive for many laboratories, but centralized handling of the tough problems in specialized facilities already seems feasible.

3A.6. PROPOSED MECHANISMS AND MODELS

Theoretical investigations date back to efforts devoted to the understanding of plasma desorption and other high-energy-particle–induced desorption techniques (Johnson, 1987). A basic question arises for all these methods: How can one account for the transfer of large molecules to the gas phase without fragmentation or degradation? The intriguing similarity between MALD and some other soft ionization methods is that they start with sudden energy deposition and they yield large molecules in the gas phase. Energy deposition and redistribution processes have emerged as a key factor in the description of MALD mechanisms (Vertes, 1991a; Vertes and Gijbels, 1991). Attempts have also been made to account for the energy transfer to the large molecules during their volatilization (Vertes, 1991b; Vertes and Gijbels, 1991).

A successful model must answer two major questions in connection with the laser-induced volatilization of large molecules

a. What is the nature of the laser-induced process leading to the transition from the solid phase to the gas phase?
b. How can large molecules escape fragmentation in an environment abruptly energized by the laser pulse?

These questions are equally relevant both in LITD and in MALD experiments. The rough options to answer question *a* are to invoke thermal or electronic processes. Closer inspection of the problem has produced several suggested mechanisms falling within these categories. Question *b* is specifically emphasized in the MALD situation where the matrix ions may undergo extensive fragmentation whereas the embedded large molecules desorb intact.

Extremely fast energy deposition—as is the case with laser heating—generates a strongly nonequilibrium population of energy levels in the solid. There are numerous different regimes for the relaxation of these energy distributions. The models suggested for the different regimes of laser desorption all incorporate some hypothesis as to the nature of this energy redistribution process.

3A.6.1. Phase Explosion

Spinodal Decomposition. It is known from thermodynamics that condensed phases can only be superheated up to a point where homogeneous vapor nucleation becomes dominant over heterogeneous nucleation (evaporation) and the whole phase is suddenly transformed into vapor (von Allmen, 1987). A rough estimate of the corresponding temperature is $0.9 \times T_c$, where T_c is the critical temperature. This phenomenon, sometimes called *phase explosion* or *spinodal decomposition*, was referred to in the explanation of fast atom bombardment (FAB) ionization experiments (Vestal, 1983; Sunner et al., 1988). Recently, preliminary molecular dynamics simulations have shown the spinodal decomposition mechanism to be feasible in particle and laser desorption experiments (Shiea and Sunner, 1990). The molecular dynamics simulation was able to visualize strongly nonequilibrium phase transitions induced by high-energy projectiles in two-dimensional Lennard–Jones fluids. Extension of the calculations to three dimensions and to laser excitation in MALD experiments is expected.

Phonon Avalanche. In laser-induced explosive desorption (Domen and Chuang, 1987) the phonon modes of the lattice are pumped by a system of excited anharmonic oscillators, i.e., by highly excited vibrational states of the molecules. Fain and Lin (1989a,b) treated UV laser–induced nonselective desorption theoretically. In their model the adsorbate (CH_2I_2 on Al_2O_3, Ag, or Al) is excited to higher electronic states. The excitation energy is then converted into internal vibrations of the adsorbates and subsequently to phonons. These authors showed that a system of excited anharmonic oscillators can become unstable under the influence of some external force field. If the energy dissipation from the phonon modes is slower than their energy gain the number of phonons shows exponential divergence; in other

words, a phonon avalanche can be observed. The main characteristics of the model are the existence of a surface-coverage-dependent threshold laser fluence for the avalanche and the molecular nonselectivity of the desorption above the threshold. On the other hand, for desorption below the threshold their model predicted selectivity. Similar treatment of IR laser–induced desorption exhibited neither molecular selectivity nor threshold behavior and no phonon avalanche was reported (Fain et al., 1989).

3A.6.2. The Cool Plume Model

Hydrodynamic description of laser-generated plume expansion has contributed to the insight of laser–solid interaction (Vertes et al., 1988a, 1990a). Shock wave development under moderate and high irradiance conditions has been demonstrated, with kinetic energy distributions of desorbed and ablated ions successfully accounted for (Vertes et al., 1989c). A refined version of the one-dimensional model was able to handle phase transitions, surface recession, and heat conduction processes in the solid, as well as electron–neutral inverse bremsstrahlung light absorption, multiple ionization, and radiation cooling in the plume (Balazs et al., 1991).

Here we outline a scenario whereby the laser energy deposited into the solid matrix leads to heating and phase transition. The generated plume, in turn, undergoes gas dynamic expansion and exhibits cooling. The entrained large molecules are therefore also stabilized in the expansion. We also discuss hydrodynamic calculations of the plume expansion.

In general, we are interested in the density, temperature, and velocity distributions of the laser-generated plume as they develop in time. In contrast to the laser plasma generation experiments, we expect moderate temperatures during volatilization of low sublimation point matrices.

In the course of laser–solid interaction two distinct phases can be recognized. The first phase covers the period when the solid surface does not reach the phase transition temperature. In this regime material transport can be neglected and the description only accounts for generating a hot spot on the solid surface. The temperature distribution is governed by the relation between the laser heating and cooling of the spot by heat conduction:

$$\frac{\partial(\rho e)}{\partial t} = -\frac{\partial}{\partial z}\left[\kappa \frac{\partial(\rho e)}{\partial z}\right] + \alpha_{\text{solid}} I \tag{6}$$

where ρe and α_{solid} stand for the energy density and the absorption coefficient of the solid material. We have already seen a special solution of this equation for the case of a uniform penetrating source [Eq. (5)]. Because we now allow both for phase transitions in the solid and for different laser pulse profiles,

a numerical solution of this equation will be sought. This solution will be used afterward as a boundary condition for the description of plume expansion.

The second phase starts when the surface of the solid is heated above the phase transition temperature. At this stage the vapor pressure of the material becomes significant and material transport across the surface cannot be neglected. To deal with the expansion problem we have to solve a simplified set of hydrodynamic equations expressing the conservation of mass, momentum, and energy:

$$\frac{\partial[\rho]}{\partial t} = -\frac{\partial[\rho v]}{\partial z} \tag{7}$$

$$\frac{\partial[\rho v]}{\partial t} = -\frac{\partial[p + \rho v^2]}{\partial z} \tag{8}$$

$$\frac{\partial\left[\rho\left(e + \frac{v^2}{2}\right)\right]}{\partial t} = -\frac{\partial\left[\rho v\left(e + \frac{p}{\rho} + \frac{v^2}{2}\right)\right]}{\partial z} + \alpha_{\text{plume}} I \tag{9}$$

where ρ, v, p, and α_{plume} denote the density, hydrodynamic velocity, pressure, and absorption coefficient of the plume, respectively. We note that all the transport equations [Eqs. (7)–(9)] are written in one-dimensional form. Therefore, only processes along the z coordinate (perpendicular to the surface) are accounted for; i.e., radial transport is neglected in the model. Assuming a Gaussian beam profile, this approximation is valid in the center of the beam where radial gradients are vanishing. However, the relevance of the results is not altered by this restriction, because at volatilization threshold (where most of the experimental work is done) only the center of the spot is hot enough to contribute substantially to the volatilization process.

Coupling between Eqs. (7)–(9) and Eq. (6) is provided by the Clausius–Clapeyron equation for vapor pressure. Under laser desorption conditions (i.e., near threshold irradiance), the plume remains optically thin; thus, the laser absorption term in Eq. (9) can be neglected. The plume is heated only by the transfer of warm material across the interface and cooled by the expansion process. Owing to the relatively low temperatures, thermal ionization and radiative cooling are not significant factors either. Solutions of Eqs. (6)–(9) were found by a computer code developed and reported earlier (Balazs et al., 1991).

The nicotinic acid–vacuum interface was investigated under the influence of a 10 ns frequency-quadrupled Nd:YAG laser pulse (Vertes et al., 1991; Vertes, 1991b). The temporal profile of the 10^7 W/cm^2 irradiance pulse is

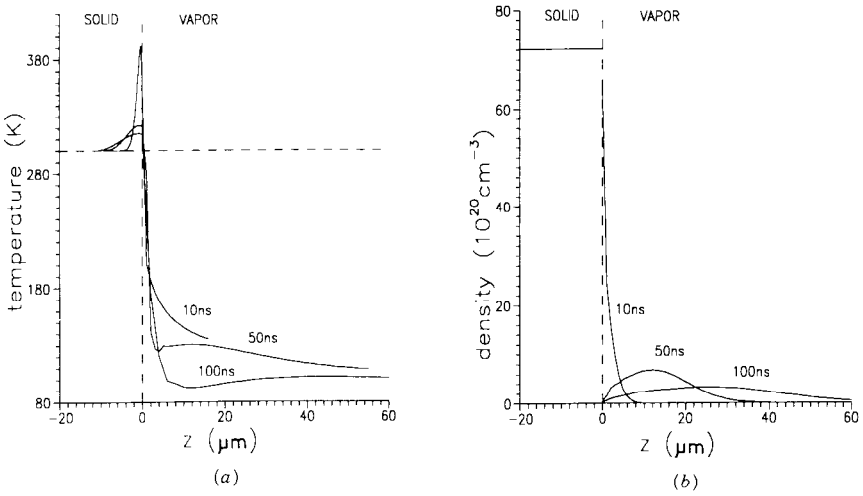

Figure 3A.11. The effect of a 10 ns frequency-quadrupled Nd:YAG laser pulse (10^7 W/cm^2) on the matrix–vacuum interface. Spatial temperature (a) and density (b) distributions are shown at different times. Surface position is marked by the vertical dashed line. In graph (a) the starting temperature is shown by the horizontal dashed line. From Vertes et al. (1991).

approximated by a square wave. Spatial distribution of the number density and temperature across the surface are shown in Figure 3A.11. Three different time stages are depicted in order to visualize postpulse behavior.

The spatial density profile at the end of the laser pulse (10 ns) showed monotonous decay (Figure 3A.11b). Subsequent cooling of the surface lowered the rate of evaporation precipitously. Consequently, the density immediately above the target dropped quickly and the vapor detached from the surface to produce a drifting and expanding plume packet (25 ns, 50 ns). We estimated the kinetic energy of particles stemming from plume translation. The drift velocity of the plume center of mass is $v_{\text{drift}} = 340$ m/s at 70 ns. Drift velocity measurements of neutrals desorbed from ferrulic acid matrix due to a 10^7 W/cm^2, 266 nm laser pulse show velocity maxima between 300 and 400 m/s (Huth-Fehre and Becker, 1991). This is surprisingly good agreement. If this result is converted to kinetic energy ($E_{\text{kin}} \approx 60$ meV), it is also a value close to the measured energies of molecules in the plume: $E_{\text{kin}} = 40$ meV (2×10^6 W/cm^2, 248 nm, tryptophan target) (Spengler et al., 1988).

It is worthwhile to note that the plume density was relatively high; at the 50 ns time stage the maximum density still exceeded one-tenth of the solid density. With further expansion of the vapor cloud the density dropped quickly. The high initial plume density has important repercussions on the

possibility of gas phase processes. It seems feasible that certain reactions are induced in this dense cloud of particles. Most important among them can be protonation, alkalination, and adduct ion formation of the guest molecules. Indeed, there is clear experimental evidence that the appearance of sodium- and/or potassium-containing quasi-molecular ions is bound to the presence of sodium and/or potassium ion signals and to the generation of a dense plume (Claereboudt et al., 1991).

Integrating the density distributions along the z-axis provides a measure of the total desorbed amount from unit surface. In Figure 3A.12 the laser irradiance dependence of this quantity is depicted. Two interesting features of this figure are the existence of a threshold irradiance and the power law relationship. Comparing Figures 3A.4 and 3A.12 positive correlation can be established between the cool plume model and measurements. Measured laser irradiance thresholds for ion production are around 2×10^6 W/cm^2, whereas calculated plume formation thresholds are close to 3×10^6 W/cm^2. The measured ion yield, Y_i, shows power law dependence on the laser irradiance: $Y_i \propto I^6$. Integrated plume density distributions, Y_n, from the model exhibit power law dependence on laser irradiance as well, but the exponent is somewhat higher: $Y_n \propto I^{7.6}$. Parametric studies of matrix properties also show strong correlation between phase transition temperature and plume density.

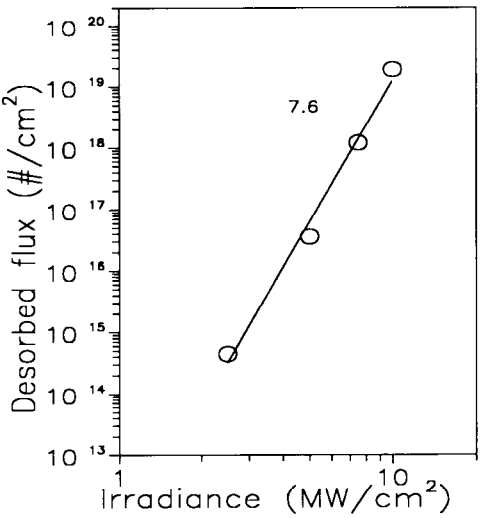

Figure 3A.12. Calculated desorbed flux of matrix molecules as a function of laser irradiance (nicotinic acid matrix; 4 × ω Nd:YAG laser). The cool plume model predicts power law with 7.6 exponent.

Another interesting feature of the plume is the spatial and temporal variation of the temperature. The surface of nicotinic acid heats up to the phase transition temperature, but quick decay of plume temperature is observed with increasing distance from the surface (Fig. 3A.11a). The actual value of the temperature drops well below room temperature due to expansion cooling. The obvious consequence of such cooling would be a stabilizing effect for the entrained large molecules. The situation is reminiscent of two-laser experiments in which jet cooling of large molecules is introduced between the desorption and ionization step.

Experimental verification of low or moderate plume temperatures, with thermally labile molecules being used as "molecular thermometers," was reported earlier (Claereboudt et al., 1991). Measuring laser-induced thermal decomposition processes of thermally extremely labile substances in native phase and in the presence of nicotinic acid matrix indicated the participation of a cooling mechanism if the matrix was present. Aryltriphenylphosphonium halide guest molecules were used as molecular thermometers in typical MALD experiments. The mass spectra revealed no thermal decomposition and low internal energies of the guest molecules, thereby supporting the cool plume model.

3A.6.3. Desorption Induced by Electronic Transitions

Low-energy electrons or UV photons may excite the surface adsorbate complex to a repulsive antibonding electronic state. A possible relaxation of this excitation is the departure of the adsorbate from the surface. The desorption induced by electronic transition (DIET) mechanism has been discovered and rediscovered several times (Menzel and Gomer, 1964; Antoniewicz, 1980). A relatively new development in utilizing the DIET model is its application to bulk etching of organic polymers by far-UV radiation (Garrison and Srinivasan, 1984, 1985). In the framework of this DIET model it is possible to rationalize polymer ablation without melting or any other thermal effect. In the irradiated volume of the polymer the monomer units are thought to be instantaneously excited to the repulsive state and leave the bulk of the solid with coherent motion.

Investigation of desorption processes induced by low-energy electron impact has already led to the idea of repulsive state participation in the mechanism of detachment (Menzel and Gomer, 1964; Antoniewicz, 1980). If by electron impact or by the absorption of UV photons an adsorbed molecule is excited electronically, the resulting state can be an antibonding state, a higher laying excited state, or an ionized state. Because of the Franck–Condon principle these excited states are not in their equilibrium geometry. The adsorbates in these configurations are frequently in the repulsive range of the interaction potential.

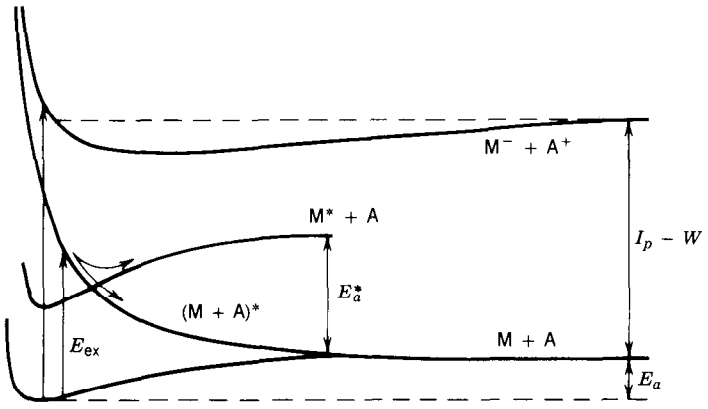

Figure 3A.13. Development of laser-induced desorption from a metallic surface (M) via repulsive states. The adsorbate (A)–surface interaction can be electronically excited to a repulsive state. Decay to M + A desorbed state or intersystem crossing to the hypersurface of the M* + A system can be observed. Higher excitation energy or two-photon processes may provide enough energy for ion desorption: $M^- + A^+$.

In Figure 3A.13 we schematically depict how the system will behave in the case of electronic excitation. If the antibonding state is reached, the adsorbed particle will experience a monotonous repulsive field and leave the surface with $(E_{ex} - E_a)$ kinetic energy, where E_{ex} and E_a are the excitation and adsorption energies, respectively. If the antibonding potential surface is intersected by the potential surface of a bonding excited state, intersystem crossing may occur and the adsorbate can be retarded. Ion desorption is observed in the case of excitation to even higher electronic states, generally attained by multiphoton processes.

It is the peculiarity of this completely nonthermal mechanism that in case of coherent electronic excitation the energy conversion leads to coherent translational motion of the desorbed particles. As a result, melting of the surface layer is avoided and extremely well-defined pits are produced. The removed particles exhibit velocity distributions oriented strongly toward the surface normal (Garrison and Srinivasan, 1985).

Microscopic modeling of laser ablation by molecular dynamic simulation supports the feasibility of this mechanism, especially for far-UV radiation (Garrison and Srinivasan, 1984, 1985). Ab initio density functional calculations and effective medium theory reveal finer details of the adsorbate–surface interaction and its perturbation by electronic excitation (Avouris et al., 1988). It is shown that the desorption of ions from metal surfaces is largely enhanced by the screening of the image charge in the metal. There are similarities between UV laser etching and the UV-MALD experiment. The recently

demonstrated possibility of IR-MALD, however, seems to be in contradiction to the basic assumptions of the DIET mechanism. Also, in the framework of this model, multicharged ions remain strongly bounded to the surface, a prediction not supported by experiments with large adsorbed molecules (Hillenkamp, 1989).

Energy distribution measurements of desorbed ions and neutrals show a marked difference in the translational energy of the two species (Spengler et al., 1988; Beavis and Chait, 1991b; Huth-Fehre and Becker, 1991). Neutrals have kinetic energies in the order of 0.1 eV, whereas the ions exhibit at least 10 times higher values. If the desorption is attributed to electronic transitions, it is straightforward to rationalize this difference. The neutrals can be desorbed by single-photon excitation to a repulsive state, whereas the ions are the result of a two-photon process leading to the ionic state (Figure 3A.13). The amount of kinetic energy of desorbing particles is a function of the potential surface shape and the excitation energy. Excitation to the steep repulsing part of the ionic state interaction potential may result in departing energetic ions.

3A.6.4. The Pressure Pulse Mechanism

Disintegration via Mechanical Stress and Shock. Another way that disintegration occurs is by thermally induced mechanical stress (Beavis et al., 1988) and shock (Lindner and Seydel, 1985). The energy absorbed from the laser pulse causes inhomogeneous heating of the sample. Thermal expansion of the illuminated region produces mechanical stress. Even at moderate laser irradiances the thermally induced stress, σ, may exceed the critical stress value, σ^*, where cracks are formed and mechanical fragmentation occurs. In principle, crack formation can be observed if the strain energy exceeds the energy of new surfaces created by the cracks. It is also possible to prove that upon mechanical fragmentation a large number of quite small fragments are formed (Vertes and Levine, 1990); therefore, many of the embedded guest molecules can be released into the gas phase.

The condition that must be met for intact large molecules to be released by thermally induced stress and crack formation is

$$\tau(\sigma = \sigma^*) \ll \tau(T_G \gg T_0) \tag{10}$$

where $\tau(T_G \gg T_0)$ is the time needed for the guest temperature to depart substantially from the initial temperature of the system, T_0.

In Figure 3A.14 the time history of crack formation is shown for a sample containing large molecules embedded in alkali halide matrix. Because of the long pulse duration of the applied CO_2 laser (10 μs), energy exchange has

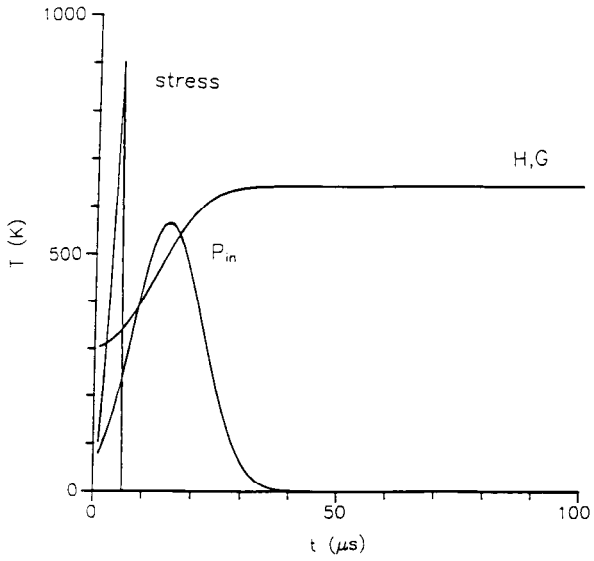

Figure 3A.14. Temporal evolution of host (H) and guest (G) temperature and thermally induced stress for a CO_2 laser pulse. The pulse profile vs. time is labeled P_{in}. The stress curve is $1000(\sigma/\sigma^*)$, where σ^* is the critical stress. At $\sigma = \sigma^*$ the matrix fragments, releasing some part of the guest molecules. From Vertes and Levine (1990) with permission of Elsevier Science Publishers B.V.

already become complete between host and guest molecules by the beginning of the excitation. The energy deposition by the laser pulse, P_{in}, generates rapidly rising thermal stress, which reaches the critical value before the overall temperature can rise excessively.

The material parameters that determine the instance of crack formation are the light absorption coefficient, the volume thermal expansion coefficient, the bulk modulus, and the critical stress value. In order to achieve earlier crack formation and guest molecules liberated with lower internal energy content, modifications are needed to increase the volume thermal expansion coefficient and/or the bulk modulus of the sample or to decrease the critical stress value. In terms of this model it is feasible that the introduction of fine metal powder into the sample improves the efficiency of volatilization (Beavis et al., 1988).

Another mechanism of releasing large molecules by mechanical effects is shock-wave-induced desorption. It has been proved that laser pulses at elevated irradiances generate shock waves in the ablated plume and compression waves in the solid target (Vertes et al., 1988a, 1989c). If a slab-like sample is

thick enough not to be perforated by the laser pulse but thin enough to experience the effect of the compression wave at the back surface, intact large molecules can be detached from the sample (Lindner and Seydel, 1985). The description of this phenomenon is complex and beyond the scope of the present discussion.

Pressure Pulse Model. Originally the pressure pulse model was developed for fast heavy-ion-induced sputtering (Johnson and Sundqvist, 1991; Johnson et al., 1991). In this model the penetrating primary particles deposit their kinetic energy into the solid and set up a pressure gradient. Upon exceeding a threshold value this pressure gradient drives the expansion of the surface layer leading to desorption. A similar scenario is envisaged for laser desorption. As the laser light penetrates the target, energy is deposited and pressure gradient builds up. This model also predicts the existence of a fluence threshold. The value of the threshold fluence depends on the amount of deposited energy converted into expansion, on the cohesive energy of the solid, and on energy transfer rates in the solid. According to this description the fluence threshold should change with varying laser pulse length. Therefore, a critical test of the model may be performed by using picosecond and nanosecond laser pulses to desorb large molecules from the same matrix (Johnson and Sundqvist, 1991).

3A.6.5. Energy Redistribution Processes

Heating of the matrix lattice by the laser pulse gives no satisfactory explanation of all the findings of UV-MALD experiments. In contrast to the presence of intact guest molecules in the plume, host fragments can be abundant in the mass spectrum. This observation points to the importance of exploring the possible energy transfer pathways in the system. In the UV-MALD experiments, primary energy deposition leads to electronic excitation of the host molecules ($\pi \rightarrow \pi^*$ transition in the case of nicotinic acid matrix) (Irinyi and Gijbels, 1992). Quick internal conversion processes lead to vibrationally highly excited ground states. Part of the host molecules will decompose from these vibrational states, but another part transfers its energy to the lattice. Thus, the lattice is heated and the phase transition temperature can eventually be reached.

Vibrational Energy Transfer Experiments. Intramolecular and intermolecular vibrational energy transfer in condensed phases has been studied by picosecond laser spectroscopic methods (Seilmeier and Kaiser, 1988). These investigations were aimed at elucidating vibrational energy redistribution and equilibration after ultrashort light pulse excitation of 10 ps duration and

less. Large organic molecules (usually dyes) dissolved in low-molecular-weight organic liquids exhibit the following features:

a. If excited above $1000\,cm^{-1}$, they often redistribute the excess energy over the vibrational manifold of the electronic ground state with a relaxation time shorter than 1 ps. It has also been shown that the transient internal temperature of the excited molecule is a meaningful term.
b. Intermolecular energy transfer is also very fast and has a relaxation time of about 10 ps, largely dependent on the degree of excitation and on the solvent molecules.
c. Excitation to high vibrational states of the S_0 ground state may exhibit fast relaxation to the bottom of the first electronically excited state (S_1). Vibrational redistribution of the energy in S_0 and in S_1 has relaxation times on the order of 0.5 ps.

Similar studies were carried out on suface adsorbates (Heilweil et al., 1989).

From our point of view such investigations should have a slightly different emphasis. First of all, in LITD or in MALD the energy is dumped into the solid substrate or into the matrix, not into the large molecule. Therefore, reverse flow of energy is generated and should be studied. Second, the amount of deposited energy is deliberately set to levels where desorption and/or phase disintegration occur; therefore, highly anharmonic displacements are induced. We cited the foregoing studies because they indicate the possibility of time-resolved energy transfer experiments of a similar nature. Scarce reports of vibrational temperature measurements on molecules after laser evaporation from a cryogenic matrix show vibrational cooling down to $T = 170 \pm 30\,K$ (aniline in CO_2 matrix; Nd:YAG laser; $3 \times 10^8\,W/cm^2$) (Elokhin et al., 1990). Under somewhat different conditions, similar temperatures were also indicated by the *cool plume model* (see Section 3A.6.2).

Desorption vs. Fragmentation in LITD. There is a long history of investigating desorption and fragmentation kinetics at different heating rates (Beuhler et al., 1974; Deckert and George, 1987). The microscopic dynamics of energy transfer from a rapidly heated surface to the adsorbate species has been treated by stochastic trajectory modeling on a computer (Lucchese and Tully, 1984; Lim and Tully, 1986), by classical molecular dynamics simulation (Holme and Levine, 1989), and by evaluation of the survival probability of adsorbates without degradation (Muckerman and Uzer, 1989; Zare and Levine, 1987). All these studies arrived at similar conclusions: if the surface heating is rapid enough the desorbing species may have considerably lower temperature than the surface itself. In the case of the frequency mismatch

between the physisorption bond and the chemical bonds of adsorbate, an energy transfer bottleneck is formed (Zare and Levine, 1987). The bottleneck model in its original form was suitable to explain LITD but not MALD experiments.

The Homogeneous Bottleneck Model. What prevents guest molecules from heating up in an environment where host molecules and lattice vibrations are both highly excited? The homogeneous bottleneck model (HBM), proposed for the description of MALD of large molecules, suggests that there is an obstacle in the energy transfer toward the embedded guest molecules. This so-called energy transfer bottleneck is caused by mismatch between the guest–host interaction frequency and the internal vibrational frequencies of the guest molecule. A simple kinetic model of the energy transfer processes shows that at an appropriately high sublimation rate the guest molecules will be liberated internally cold (Vertes et al., 1990a; Vertes and Levine, 1990).

In order to follow the path of the deposited energy in the target we partition its energy density, ρe, in the following way:

$$\rho e = (1 - x)H + L + xG + B \tag{11}$$

where H, L, G, and B denote the energy density content of the host, the lattice, and the guest and energy density used for bond breaking, respectively; x is the volume fraction of the guest molecules.

We take the area of the volume element heated by the laser to be determined by the laser beam cross section and its thickness by the inverse of the host absorption coefficient, α_{0H}^{-1}. The energy density is increased in this volume by laser heating:

$$\frac{d(\rho e)_{\text{heat}}}{dt} = \frac{\alpha_{0H} + \alpha_{0G}}{\pi^{1/2}} I_0 \exp\left[-\frac{(t - t_0)^2}{\tau_p^2} \right] \tag{12}$$

Here, I_0 stands for the laser irradiance; t_0 and τ_p describe the center and the half-width of a Gaussian laser pulse; and α_{0H} and α_{0G} are the effective absorption coefficients of the host and guest (weighted by their concentration).

In the power density regime we are discussing, there are two main mechanisms to cool the excited volume: phase transformation and heat conduction. Inspecting the enthalpies of the possible phase transition processes, we conclude that the two most effective cooling phase transitions are evaporation and sublimation.

The cooling rate, expressed by the phase transition enthalpy, ΔH_{phtr}, and

temperature, T_{phtr} is written as

$$\frac{d(\rho e)_{\text{cool}}}{dt} = \frac{\alpha_{0H} p_0 \Delta H_{\text{phtr}}}{(2\pi M R T)^{1/2}} \exp\left[\frac{\Delta H_{\text{phtr}}(T_L - T_{\text{phtr}})}{R T_L T_{\text{phtr}}}\right] \tag{13}$$

where p_0, is the ambient pressure; T_L is the lattice temperature expressed by $T_L = V_M L / C_p$; V_M and C_p are the molar volume and the lattice specific heat of the host with molecular weight M.

To follow the energy redistribution processes we introduce the kinetic equations where the energy exchange terms are proportional to the energy differences (Vertes et al., 1990a):

$$\frac{dH}{dt} = \frac{\alpha_{0H}}{\alpha_{0H} + \alpha_{0G}} \frac{d(\rho e)_{\text{heat}}}{dt} - \alpha_{HL}(H - L) - \alpha_{HG}(H - G) - \alpha_{HB} H \tag{14}$$

$$\frac{dL}{dt} = \alpha_{HL}(H - L) - \alpha_{LG}(L - G) - \frac{d(\rho e)_{\text{cool}}}{dt} \tag{15}$$

$$\frac{dG}{dt} = \frac{\alpha_{0G}}{\alpha_{0H} + \alpha_{0G}} \frac{d(\rho e)_{\text{heat}}}{dt} + \alpha_{HG}(H - G) + \alpha_{LG}(L - G) - \alpha_{GB} G \tag{16}$$

$$\frac{dB}{dt} = \alpha_{HB} H + \alpha_{GB} G \tag{17}$$

Here, α_{HL}, α_{HG}, α_{HB}, α_{LG}, and α_{GB} are the host–lattice, host–guest, host-bond-breaking, lattice–guest, and guest-bond-breaking energy transfer coefficients, respectively. It is assumed that all the processes except bond breaking are reversible.

The physical picture of laser volatilization underlying these equations is the following. The laser radiation electronically excites mostly the host and, with a lower cross section, also the guest molecules. With very fast internal conversion processes (on the picosecond time scale) the electronic excitation leads to internal vibrational excitation. At a given rate (α_{HL}) these internal vibrations are transferred to lattice vibration and are also channeled directly to guest vibrations (α_{HG}). The lattice is cooled by the phase transformation and transfers energy to the guest molecules (α_{LG}). The guest heating rate is determined by direct light absorption and energy transfer from the lattice and from the host molecules. Both the host and the guest molecules are subject to irreversible fragmentation, which consumes some part of the energy. An energy transfer bottleneck is an extremely low value of one or more of the transfer coefficients.

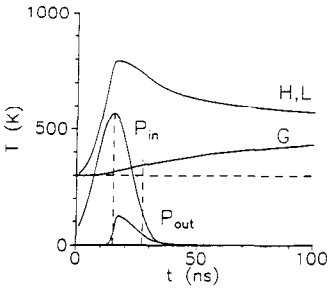

Figure 3A.15. Energy pathways for UV laser irradiation of nicotinic acid matrix containing 10^{-4} volume fraction of an $M_G = 10^5$ protein; P_{in} and P_{out} are the laser power input and the power output carried by sublimation per unit matrix area, respectively. See text for further details. From Vertes et al. (1990a) courtesy of John Wiley & Sons, Ltd.

In Figure 3A.15 the time development of host (H) and guest (G) internal temperatures are shown. The laser power input, P_{in}, heats up the host molecules. The lattice temperature is proved to be identical with the host temperature. Here P_{out} shows the power drained from the system by phase transition, in this case by sublimation. Inspecting Figure 3A.15 we note that near the maximum desorption rate the guest molecules are still close to their initial temperature. Thus, in this model, the possibility of volatilizing internally cold large molecules has been demonstrated. Recent experiments show that the matrix-assisted method is not bound to desorption from thin layers adsorbed on a substrate. In accordance with the predictions of the HBM theory, it can be carried out without substrate, from suspended crystals (Vertes et al., 1990b).

The criterion for liberating internally cold molecules from a strongly absorbing matrix can be expressed in a very general form:

$$\tau(T_L = T_{subl}) \ll \tau(T_G \approx T_H) \tag{18}$$

where $\tau(T_L = T_{subl})$ is the time required to reach sublimation temperature, T_{subl}, by the lattice temperature, T_L, and $\tau(T_G \approx T_H)$ is the approximate time needed to reach the equality of T_H and T_G, the host and the guest temperature.

The key material factors in the model appear to be the low heat of sublimation, subcritical concentration of the guest molecules, and the irradiance input in a short time compared to the sublimation induction period (Vertes et al., 1990a). The model is homogeneous in that the energy density is taken to be uniform within the "hot region" of the matrix. The two competing effects are the rates of energy transfer from the matrix to the guest molecules and the desorption by sublimation. It is the bottleneck for energy transfer to the embedded guest molecules that makes their energy content lag behind that of the matrix. This is particularly so for an initially cold sample. When a sufficiently high rate of sublimation can be achieved, the guest molecules (or adduct ions) will desorb internally cold and will thus not fragment.

This simple competitive kinetic model is able to reproduce several experimental findings: the existence of a laser irradiance threshold and its estimated value; the suitability of matrices with low phase transition temperatures; the low volume concentration requirement for the large molecules; and the need for a short laser pulse, i.e., for fast heating rates. It also predicts that sample cooling should extend the possibilities of the method. A generalization of the idea involved in MALD suggests that new desorption techniques can be successful if the liberation of large molecules by phase disintegration precedes their destruction by fragmentation (Vertes, 1991a).

There are unanswered questions in all the models discussed above. None of the models accounts for ion formation—a prerequisite for mass analysis and detection in mass spectrometry. A further shortcoming of these theories is that none of them explains the large differences in efficiency between matrices with similar phase transition temperatures and optical characteristics (Beavis and Chait, 1990c).

3A.7. ION FORMATION

The origin of the ions in the system is a subject of continuing debate. It is clear from postionization experiments that the degree of ionization in the plume is very low. In light of the calculated temperature values, it is also obvious that thermal ionization is not a feasible ion production mechanism. Rather, protonation and other adduct ion formation mechanisms shall be regarded as the primary source of ions. These processes can be discussed in terms of preformed ion volatilization and gas phase ion formation. Guest particles that are already in their ionized form in the solid state (preformed ions) can give rise to gas phase ions extremely easily. Molecular ions of these substances in MALD experiments were produced even without ion production from the matrix (Claereboudt et al., 1991). These findings support the suggestion that the role of the matrix is to embed and separate the guest particles in the solid phase and to entrain them in the course of volatilization.

Ion formation mechanisms can be classified according to the ion formation site and according to the process involved. Certain molecular solids are built up of ion associates. For example, nicotinic acid—a frequently used matrix in MALD experiments—is built up of molecular dimers held together by charge disproportionation. Defects and impurities are also sources of ionized particles. Surface states and adsorption itself are frequently promoting ion formation by preforming the gas phase ion. However, gas phase processes can also be effective in producing the ionized species. Electron impact ionization and ion–molecule reactions have high cross sections, and the ions

generated in the gas phase are directly collected by the accelerating field of the spectrometer.

Thermal ion formation is not likely in the case of large molecules because the required temperatures would certainly destruct these molecules. Photoprocesses are very inefficient for IR radiation but are worthy of some interest in UV experiments. Indeed, two photons of the most often used frequency-quadrupled Nd:YAG laser provide enough energy to ionize many organic molecules.

Inspecting MALD spectra tells us that the most favored channel of molecular ion formation is cationization. Protonated and/or alkalinated molecular ions are usually abundant in positive ion spectra. Not much is known about the formation of these ions. It seems likely that protonated ions are already formed on the surface or even in the solid phase by proton hopping (Kammer, 1990) and alkalinated ions are mostly the products of gas phase ion–molecule reactions (van der Peyl et al., 1982b).

In the case of negligible dipole moments ion–molecule reactions are described by the Gioumousis–Stevenson theory (see Gioumousis and Stevenson, 1958). A simple rate constant expression can be derived for the case of the cationization of a very large molecule by a relatively light ion ($M_2 \ll M_1$):

$$k = 2\pi e\left(\frac{\alpha_{\text{pol}}}{M_2}\right)^{1/2} \tag{19}$$

where α_{pol} and M_2 are the polarizability of the large molecule and the mass of the light ion, respectively. Evaluation of Eq. (19) indicates that protonation is six times faster than the reaction with K^+ if the concentrations are similar. Calculations of the desorption profiles and ion–molecule reaction rates show feasible ion production rates for small molecules also (Vertes et al., 1988b, 1989d). However, Eq. (19) predicts moderate deterioration of gas phase cationization with increasing ion mass.

There are other types of ions abundant in the high-mass region. Adduct ions are formed by the combination of the high-mass molecules with fragment ions of the matrix. Their origin is probably also a gas phase ion–molecule process. Multiply charged species are easy to form from large molecules, as is learned from electrospray ionization experiments. Because of the possibility of independent ionization at different sites of the molecule and because of distant charge locations, the increasing size can be accompanied by increasing number of charges. Ionized clusters quite often appear in the spectra. It is unlikely that these clusters are formed in the gas phase, for guest molecule concentration is already very low in the matrix. Most experiments are performed on peptides and on proteins. These compounds are amphoteric

in character and readily associate in solution. In principle the associates can survive sample preparation and desorb as a single particle.

Because only a small fraction of the desorbed species is ionized, increasing ionization efficiency might well produce significant improvement in detection limits and an even broader range of applications. Clearly, more work is needed to enhance our understanding of laser-induced ion formation from large molecules.

ACKNOWLEDGMENTS

One of the authors (A. V.) is indebted to the National Science Foundation (Grant # CTS-9212389) and to the George Washington University Facilitating Fund for their support.

REFERENCES

Allen, M. H., Grindstaff, D. J., Vestal, M. L., and Nelson, R. W. (1991). *Biochem. Soc. Trans.* **19**, 954–957.

Antoniewicz, P. R. (1980). *Phys. Rev. B* **21**, 3811–3815.

Avouris, P., Kawai, R., Lang, N. D., and Newns, D. M. (1988). *J. Chem. Phys.* **89**, 2388–2396.

Balazs, L., Gijbels, R., and Vertes, A. (1991). *Anal. Chem.* **63**, 314–320.

Barber, M., and Green, B. N. (1987). *Rapid Commun. Mass Spectrom.* **1**, 80–83.

Beavis, R. C., and Chait, B. T. (1989a). *Rapid Commun. Mass Spectrom.* **3**, 233–237.

Beavis, R. C., and Chait, B. T. (1989b). *Rapid Commun. Mass Spectrom.* **3**, 432–435.

Beavis, R. C., and Chait, B. T. (1989c). *Rapid Commun. Mass Spectrom.* **3**, 436–439.

Beavis, R. C., and Chait, B. T. (1990a). *Anal. Chem.* **62**, 1836–1840.

Beavis, R. C., and Chait, B. T. (1990b). *Proc. 38th ASMS Conf. Mass Spectrom. Allied Top., Tucson, Arizona, 1990*, pp. 26–27.

Beavis, R. C., and Chait, B. T. (1990c). *Proc. 38th ASMS Conf. Mass Spectrom. Allied Top., Tucson, Arizona, 1990*, pp. 152–153.

Beavis, R. C., and Chait, B. T. (1990d). *Proc. Natl. Acad. Sci.* USA **87**, 6873–6877.

Beavis, R. C., and Chait, B. T. (1991a). In *Methods and Mechanisms for Producing Ions from Large Molecules* (K. G. Standing and W. Ens, eds.), pp. 227–234. Plenum, New York.

Beavis, R. C., and Chait, B. T. (1991b). *Chem. Phys. Lett.* **181**, 479–484.

Beavis, R. C., Lindner, J., Grotemeyer, J., and Schlag, E. W. (1988). *Z. Naturforsch.* **43a**, 1083.

Becker, C. H., Jusinski, L. E., and Moro, L. (1990). *Int. J. Mass Spectrom. Ion Processes* **95**, R1–R4.

Beuhler, R. J., Flanigan, E., Greene, L. J., and Friedman, L. (1974). *J. Am. Chem. Soc.* **96**, 3990–3999.

Boernsen, K. O., Schaer, M., and Widmer, H. M. (1990). *Chimia* **44**, 412–416.

Boernsen, K. O., Schaer, M., Gassmann, E., and Steiner, V. (1991). *Biol. Mass Spectrom.* **20**, 471–478.

Castoro, J. A., Koster, C., and Wilkins, C. (1992). *Rapid Commun. Mass Spectrom.* (in press).

Chait, B. T., Wang, R., Beavis, R. C., and Kent, S. B. H. (1992). *Proc. 40th ASMS Conf. Mass Spectrom. Allied Top., Washington, D. C., 1992*, pp. 1939–1940.

Claereboudt, J., Claeys, M., Gijbels, R., and Vertes, A. (1991). *Proc. 39th ASMS Conf. Mass Spectrom. Allied Top., Nashville, Tennessee, 1991*, pp. 322–323.

Daves, G. D., Jr. (1979). *Mass Spectrom.* **12**, 359–365.

Deckert, A. A., and George, S. M. (1987). *Surf. Sci. Lett.* **182**, 215.

Domen, K., and Chuang, T. J. (1987), *Phys. Rev. Lett.* **59**, 1484–1487.

Elokhin, V. A., Krutchinsky, A. N., and Ryabov, S. E. (1990). *Chem. Phys. Lett.* **170**, 193–196.

Ens, W., Mao, Y., Mayer, F., and Standing, K. G. (1990). *Proc. 38th ASMS Conf. Mass Spectrom. Allied Top., Tucson, Arizona*, pp. 24–25.

Ens, W., Mao, Y., Mayer, F., and Standing, K. G. (1991). *Rapid Commun. Mass Spectrom.* **5**, 117–123.

Fain, B., and Lin, S. H. (1989a). *Chem. Phys. Lett.* **157**, 233–238.

Fain, B., and Lin, S. H. (1989b). *J. Chem. Phys.* **91**, 2726–2734.

Fain, B., Lin, S. H., and Gortel, Z. W. (1989). *Surf. Sci.* **213**, 531–555.

Fenn, J. B., Mann, M., Meng, C. K., Wong, S. F., and Whitehouse, C. M. (1990). *Mass Spectrom. Rev.* **9**, 37–70.

Finnigan MAT (1991). *Analytical Biochemistry*, LASERMAT Appl. Data Sheet No. 5. San Jose, CA.

Frey, R., and Holle, A. (1990). *Proc. 38th ASMS Conf. Mass Spectrom. Allied Top., Tucson, Arizona, 1990*, pp. 212–213.

Gabius, H. J., Bardosi, A., Gabius, S., Hellmann, K. P., Karas, M., and Kratzin, H. (1989). *Biochem. Biophys. Res. Commun.* **163**, 506–512.

Garrison, B. J., and Srinivasan, R. (1984). *Appl. Phys. Lett.* **44**, 849–851.

Garrison, B. J., and Srinivasan, R. (1985). *J. Appl. Phys.* **57**, 2909–2914.

Gioumousis, G., and Stevenson, D. P. (1958). *J. Chem. Phys.* **29**, 294.

Grasselli, J. G., and Ritchey, W. M., eds. (1975). *Atlas of Spectral Data and Physical Constants for Organic Compounds.* CRC Press, Cleveland, OH.

Hahn, J. H., Zenobi, R., and Zare, R. N. (1987). *J. Am. Chem. Soc.* **109**, 2842–2843.

Harada, K., Suzuki, M., and Kambara, H. (1982). *Org. Mass Spectrom.* **17**, 386–391.

Hedin, A., Westman, A., Hakansson, P., Sundqvist, B. U. R., and Mann, M. (1991). In *Methods and Mechanisms for* Producing Ions from Large Molecules (K. G. Standing and W. Ens, eds.), pp. 211–219. Plenum, New York.

Heilweil, E. J., Casassa, M. P., Cavanagh, R. R., and Stephenson, J. C. (1989). *Annu. Rev. Phys. Chem.* **40**, 143–171.

Hettich, R. L., and Buchanan, M. V. (1990). *Proc. 38th ASMS Conf. Mass Spectrom. Allied Top., Tucson, Arizona, 1990*, 156–157.

Hillenkamp, F. (1989). *Adv. Mass Spectrom.* **11A**, 354.

Hillenkamp, F. (1990). *Proc. 38th ASMS Conf. Mass Spectrom. Allied Top., Tucson, Arizona, 1990*, pp. 8–9.

Hillenkamp, F., Karas, M., Ingendoh, A., and Stahl, B. (1990). In *Biological Mass Spectrometry* (A. L. Burlingame and J. A. McCloskey, eds.), pp. 49–60. Elsevier, Amsterdam.

Hillenkamp, F., Karas, M., Beavis, R. C., and Chait, B. T. (1991). *Anal Chem.* **63**, 1193A–1203A.

Holme, T. A., and Levine, R. D. (1989). *Surf. Sci.* **216**, 587–614.

Huth-Fehre, T., and Becker, C. H. (1991). *Rapid Commun. Mass Spectrom.* **5**, 378–382.

Ijames, C. F., and Wilkins, C. L. (1988). *J. Am. Chem. Soc.* **110**, 2687–2688.

Irinyi, G., and Gijbels, R. (1992). *Proc. 4th Sanibel Conf. Mass Spectrom. ASMS, Sanibel Island, Florida, 1992*, p. 59.

Johnson, R. E. (1987). *Int. J. Mass Spectrom. Ion Processes* **78**, 357–392.

Johnson, R. E., and Sundqvist, B. U. R. (1991). *Rapid Commun. Mass Spectrom.* **5**, 574–578.

Johnson, R. E., Banerjee, S., Hedin, A., Fenyo, D., and Sundqvist, B. U. R. (1991). In *Methods and Mechanisms for Producing Ions from Large Molecules* (K. G. Standing and W. Ens, eds.), pp. 89–99. Plenum, New York.

Juhasz, P., Papayannopoulo, I. A., Zeng, C., Papov, V., and Biemann, K. (1992). *Proc. 40th ASMS Conf. Mass Spectrom. Allied Top., Washington, D.C., 1992*, pp. 1913–1914.

Kammer, H. F. (1990). In *Mass Spectrometry of Large Non-Volatile Molecules for Marine Organic Chemistry* (E. R. Hilf and W. Tuszynski, eds.), pp. 61–72. World Scientific, Singapore.

Karas, M., and Hillenkamp, F. (1988). *Anal. Chem.* **60**, 2299–2301.

Karas, M., Bachmann, D., Bahr, U., and Hillenkamp, F. (1987). *Int. J. Mass Spectrom. Ion Processes* **78**, 53–68.

Karas, M., Bahr, U., and Hillenkamp, F. (1989a). *Int. J. Mass Spectrom. Ion Processes* **92**, 231–242.

Karas, M., Bahr, U., Ingendoh, A., and Hillenkamp, F. (1989b). *Angew. Chem., Int. Ed. Engl.* **28**, 760–761.

Karas, M., Ingendoh, A., Bahr, U., and Hillenkamp, F. (1989c). *Biomed. Environ. Mass Spectrom.* **18**, 841–843.

Karas, M., Bahr, U., Ingendoh, A., Nordhoff, E., Stahl, B., Strupat, K., and Hillenkamp, F. (1990a). *Anal. Chim. Acta* **241**, 175–185.

Karas, M., Bahr, U., Ingendoh, A., Stahl, B., Strupat, K., Nordhoff, E., and Hillenkamp, F. (1990b). *Proc. 2nd Int. Symp. Appl. Mass Spectrum. Health Sci., Barcelona, Spain.*

Kaufmann, R., Spengler, B., and Kirsch, D. (1991). In *Methods and Mechanisms for Producing Ions from Large Molecules* (K. G. Standing and W. Ens, eds.), pp. 235–245. Plenum, New York.

Kaufmann, R., Kirsch, D., Rood, H., and Spengler, B. (1992). *Rapid Commun. Mass Spectrom.* **6**, 98–104.

Keough, T., Lacey, M. P., Oppenheimer, C. L., and Thaman, D. A. (1992). *Proc. 40th ASMS Conf. Mass Spectrom. Allied Top., Washington, D.C., 1992*, pp. 1907–1908.

Kratzin, H. D., Wiltfang, J., Karas, M., Neuhoff, V., and Hischmann, N. (1989). *Anal. Biochem.* **183**, 1–8.

Lax, M. (1977). *J. Appl. Phys.* **48**, 3919–3924.

Lax, M. (1978). *Appl. Phys. Lett.* **33**, 786–788.

Lim, C., and Tully, J. C. (1986). *J. Chem. Phys.* **85**, 7423–7433.

Lindner, B., and Seydel, U. (1985). *Anal. Chem.* **57**, 895–899.

Loo, J. A., Edmonds, C. G., Smith, R. D., Lacey, M. P., and Keough, T. (1990). *Biomed. Environ. Mass Spectrom.* **19**, 286–294.

Lucchese, R. R., and Tully, J. C. (1984). *J. Chem. Phys.* **81**, 6313–6319.

Martin, W. B., Silly, L., Murphy, C. M., Raley, T. J., Jr., Cotter, R. J., and Bean, M. F. (1989). *Int. J. Mass Spectrom. Ion Processes* **92**, 243–265.

Menzel, D., and Gomer, R. (1964). *J. Chem. Phys.* **41**, 3311–3328.

Mock, K. K., Davey, M., and Cottrell, J. S. (1991). *Biochem. Biophys. Res. Commun.* **177**, 644–651.

Muckerman, J. T., and Uzer, T. (1989). *J. Chem. Phys.* **90**, 1968–1973.

Nelson, R. W., and Williams, P. (1990). *Proc. 38th ASMS Conf. Mass Spectrom. Allied Top, Tucson, Arizona, 1990*, pp. 168–169.

Nelson, R. W., Rainbow, M. J., Lohr, D. E., and Williams, P. (1989). *Science* **246**, 1585–1587.

Nelson, R. W., Thomas, R. M., and Williams, P. (1990). *Rapid Commun. Mass Spectrom.* **4**, 348–351.

Nelson, R. W., McLean, M. A., and Vestal, M. L. (1992). *Proc. 40th ASMS Conf. Mass Spectrom. Allied Top., Washington, D.C., 1992*, pp. 1919–1920.

Nohmi, T., and Fenn, J. B. (1990). *Proc. 38th ASMS Conf. Mass Spectrom. Allied Top. Tucson, Arizona, 1990*, pp. 10–11.

Nuwaysir, L. M., and Wilkins, C. L. (1990). *Proc. 38th ASMS Conf. Mass Spectrom. Allied Top., Tucson, Arizona, 1990*, pp. 844–845.

Oates, M. D., and Jorgenson, J. W. (1990). *Anal. Chem.* **62**, 1577–1580.

Overberg, A., Karas, M., Bahr, U., Kaufmann, R., and Hillenkamp, F. (1990). *Rapid Commun. Mass Spectrom.* **4**, 293–296.

Philippoz, J. M., Zenobi, R., and Zare, R. N. (1989). *Chem. Phys. Lett.* **158**, 12–17.

Romano, L. J., and Levis, R. J. (1991). *J. Am. Chem. Soc.* **113**, 9665–9667.

Salehpour, M., Perera, I., Kjellberg, J., Hedin, A., Islamian, M. A., Hakansson, P., and Sundqvist, B. U. R. (1989). *Rapid Commun. Mass Spectrom.* **3**, 259–263.

Salehpour, M., Perera, I. K., Kjellberg, J., Hedin, A., Islamian, M. A., Hakansson, P., Sundqvist, B. U. R., Roepstorff, P., Mann, M., and Klarskov, K. (1990). In *Ion Formation from Organic Solids (IFOS V)* (A. Hedin, B. U. R. Sundqvist, and A. Benninghoven, eds.), pp. 119–124. Wiley, Chichester.

Schaer, M., Boernsen, K. O., and Gassmann, E. (1991a). *Rapid Commun. Mass Spectrom.* **5**, 319–326.

Schaer, M., Boernsen, K. O., Gassmann, E., and Widmer, H. M. (1991b). *Chimia* **45**, 123–126.

Seilmeier, A., and Kaiser, W. (1988). In *Ultrashort Laser Pulses and Applications* (W. Kaiser, ed.), pp. 279–317. Springer-Verlag, Berlin.

Shibanov, A. N. (1986). In *Laser Analytical Spectrochemistry* (V. S. Letokhov, ed.), pp. 353–404. Adam Hilger, Bristol.

Shiea, J., and Sunner, J. (1990). *Proc. 38th ASMS Conf. Mass Spectrom. Allied Top., Tucson, Arizona, 1990*, pp. 166–167.

Siegel, M. M., Hollander, I. J., Hamann, P. R., James, J. P., Hinman, L., Smith, B. J., Farnsworth, A. P. H., Phipps, A., King, D. J., Karas, M., Ingendoh, A., and Hillenkamp, F. (1991). *Anal. Chem.* **63**, 2470–2481.

Siggia, S. (1968). *Survey of Analytical Chemistry*, pp. 141–175. McGraw-Hill, New York.

Simpson, C. J. S. M., and Hardy, J. P. (1986). *Chem. Phys. Lett.* **130**, 175–180.

Spengler, B., and Cotter, R. J. (1990). *Anal. Chem.* **62**, 793–796.

Spengler, B., and Kaufmann, R. (1992). *Analusis* **20**, 91–101.

Spengler, B., Bahr, U., Karas, M., and Hillenkamp, F. (1988). *Anal. Instrum.* **17**, 173–193.

Spengler, B., Dolce, J. W., and Cotter, R. J. (1990a). *Anal. Chem.* **62**, 1731–1737.

Spengler, B., Pan, Y., Cotter, R. J., and Kan, L. S. (1990b). *Rapid Commun. Mass Spectrom.* **4**, 99–102.

Spengler, B., Kirsch, D., Kaufmann, R., Karas, M., Hillenkamp, F., and Giessmann, U. (1990c). *Rapid Commun. Mass Spectrom.* **4**, 301–305.

Spengler, B., Kirsch, D., and Kaufmann, R. (1991). *Rapid Commun. Mass Spectrom.* **5**, 198–202.

Spengler, B., Kirsch, D., Kaufmann, R., and Jaeger, E. (1992). *Rapid Commun. Mass Spectrom.* **6**, 105–108.

Stahl, B., Steup, M., Karas, M., and Hillenkamp, F. (1991). *Anal. Chem.* **63**, 1463–1466.

Strobel, F. H., Solouki, T., White, M. A., and Russell, D. H. (1991). *J. Am. Soc. Mass Spectrom.* **2**, 91–94.

Sundqvist, B., and Macfarlane, R. D. (1985). *Mass Spectrom. Rev.* **4**, 421–460.

Sunner, J., Ikonomou, M. G., and Kebarle, P. (1988). *Int. J. Mass Spectrom. Ion Processes* **82**, 221–237.

Tanaka, K., Waki, H., Ido, Y., Akita, S., Yoshida, Y., and Yoshida, T. (1988). *Rapid Commun. Mass Spectrom.* **2**, 151–153.

Van Berkel, G. J., Glish, G. L., and McLuckey, S. A. (1990). *Anal. Chem.* **62**, 1284–1295.

van der Peyl, G. J. Q., Haverkamp, J., and Kistemaker, P. G. (1982a). *Int. J. Mass Spectrom. Ion Phys.* **42**, 125–141.

van der Peyl, G. J. Q., Isa, K., Haverkamp, J., and Kistemaker, P. G. (1982b). *Nucl. Intrum. Methods* **198**, 125–130.

Vertes, A. (1991a). In *Methods and Mechanisms for Producing Ions from Large Molecules* (K. G. Standing and W. Ens, eds.), pp. 275–286. Plenum, New York.

Vertes, A. (1991b). In *Microbeam Analysis—1991* (D. G. Howitt, ed.), pp. 25–30. San Francisco Press, San Francisco.

Vertes, A., and Gijbels, R. (1991). *Scanning Microsc.* **5**, 317–328.

Vertes, A., and Levine, R. D. (1990). *Chem. Phys. Lett.* **171**, 284–290.

Vertes, A., Juhasz, P., DeWolf, M., and Gijbels, R. (1988a). *Scanning Microsc.* **2**, 1853–1877.

Vertes, A., Juhasz, P., Jani, P., and Czitrovszky, A. (1988b). *Int. J. Mass Spectrom. Ion Processes* **83**, 45–70.

Vertes, A., DeWolf, M., Juhasz, P., and Gijbels, R. (1989a). *Anal. Chem.* **61**, 1029–1035.

Vertes, A., Juhasz, P., Balazs, L., and Gijbels, R. (1989b). In *Microbeam Analysis—1989* (P. E. Russell, ed.), pp. 273–276. San Francisco Press, San Francisco.

Vertes, A., Juhasz, P., DeWolf, M., and Gijbels, R. (1989c). *Int. J. Mass Spectrom. Ion Processes* **94**, 63–85.

Vertes, A., Juhasz, P., and Gijbels, R. (1989d). *Fresenius' Z. Anal. Chem.* **334**, 682.

Vertes, A., Gijbels, R., and Levine, R. D. (1990a). *Rapid Commun. Mass Spectrom.* **4**, 228–233.

Vertes, A., Balazs, L., and Gijbels, R. (1990b). *Rapid Commun. Mass Spectrom.* **4**, 263–266.

Vertes, A., Gijbels, R., and Adams, F. (1990c). *Mass Spectrom. Rev.* **9**, 71–113.

Vertes, A., Irinyi, Gy., Balazs, L., and Gijbels, R. (1991). *Proc. 39th ASMS Conf. Mass Spectrom. Allied Top., Nashville, Tennessee, 1991*, pp. 927–928.

Vestal, M. (1983). *Mass Spectrom. Rev.* **2**, 447–480.

Von Allmen, M. (1987). *Laser-beam Interactions with Materials: Physical Principles and Applications.* Springer-Verlag, Berlin.

Voyksner, R. D., Williams, F. P., Smith, C. S., Koble, D. L., and Seltzman, H. H. (1989). *Biomed. Environ. Mass Spectrom.* **18**, 1071–1078.

Wedler, G., and Ruhmann, H. (1982). *Surf. Sci.* **121**, 464–486.

Wilkins, C. L., Castoro, J. A., and Koester, C. (1992). *Proc. 40th ASMS Conf. Mass Spectrom. Allied Top., Washington, D. C., 1992*, pp. 1923–1924.

Williams, P. (1990). In *Ion Formation from Organic Solids (IFOS V)* (A. Hedin, B. U. R. Sundqvist, and A. Benninghoven, eds.), pp. 131–135. Wiley, Chichester.

Williams, P., and Nelson, R. W. (1990). *Proc. 38th ASMS Conf. Mass Spectrom. Allied Top, Tucson, Arizona, 1990*, pp. 22–23.

Yip, T. T., and Hutchens, T. W. (1992). *Proc. 40th ASMS Conf. Mass Spectrom. Allied Top., Washington, D. C., 1992*, pp. 1915–1916.

Zare, R. N., and Levine, R. D. (1987). *Chem. Phys. Lett.* **136**, 593–599.

Zare, R. N., Hahn, J. H., and Zenobi, R. (1988). *Bull. Chem. Soc. Jpn.* **61**, 87–92.

Zenobi, R., Hahn, J. H., and Zare, R. N. (1988). *Chem. Phys. Lett.* **150**, 361–365.

Zhao, S., Somayajula, K. V., Sharkey, A. G., and Hercules, D. M. (1990a). *Proc. 38th ASMS Conf. Mass Spectrom. Allied Top., Tucson, Arizona, 1990*, pp. 154–155.

Zhao, S., Somayajula, K. V., Sharkey, A. G., and Hercules, D. M. (1990b). *Fresenius, Z. Anal. Chem.* **338**, 588–592.